JOURNAL OF PROPULSION AND POWER
Vol. 24, No. 6, November–December 2008

Atmospheric Cruise Flight Challenges for Hypersonic Vehicles Under the Ajax Concept

Alexander Kuranov* and Alexey Korabelnikov†
Leninetz Holding Company, 196066, St. Petersburg, Russia

DOI: 10.2514/1.24684

The challenges of atmospheric cruise flight of a hydrocarbon-fueled hypersonic flight vehicle under the Ajax concept are discussed in this paper. Particular emphasis has been placed on innovative technologies of mastering hypersonic flight velocities that provide for the creation of active thermal protection as well as a magneto-plasmachemical engine. Thermal protection ensures not only cooling of construction, but also production of a hydrogenous mixture, improving combustion behavior. The magnetohydrodynamic effect on the flow makes it possible to enhance the specific impulse of the engine and to create a controllable inlet under an offdesign flight condition. The expediency of magnetohydrodynamic generator application onboard a hypersonic flight vehicle as a power source has also been demonstrated.

I. Introduction

ONE of the avenues for aeronautical technology evolution is the creation of hypersonic flight vehicles (HFVs) capable of sustained cruise flight in the atmosphere. The quest for flight altitude increase up to 30–40 km leads to velocities exceeding Mach 6.0. Such conditions of flight enable the realization of many scientific, economic, military, and other tasks for which neither modern-day aeronautics nor astronautics present necessary solutions. In addition, combat HFVs (airplanes and cruise missiles) would be highly invulnerable under such flight conditions.

The concept of hypersonic flight vehicles in development under the name Ajax [1,2] at the Leninetz Holding Company is based on the active energy interaction of the system with the airflow past it. An HFV of the Ajax concept is an open aerothermodynamic system. Kinetic energy of the hypersonic airstream assimilated by HFV subsystems is transformed into a wide spectrum of useful activities. Such an approach lends an opportunity to crucially remodel all aspects of further development of the aeronautical and aerospace technologies. Active structure cooling should be realized using steam reforming of the regular hydrocarbon aviation fuel, which in itself is the basic energy carrier. The resulting (after hydrocarbon decomposition) hydrogen is used for improvement of fuel-mixture parameters. Hydrogen production and magnetohydrodynamic (MHD) system applications for airflow stagnation and acceleration open the way for the creation of a scramjet. The power achieved in the process significantly exceeds that of the existing systems. The electric energy produced can be used in plasma flow over systems for increasing HFV aerodynamic efficiency.

Within the framework of the Ajax conception, new technologies aimed at mastering hypersonic flight velocities have been suggested [3]. Their application could enable the creation of HFV active thermal protection and a fuel-conversion system based on chemical-heat regeneration, magnetoplasmachemical engine (MPCE) exerting a power effect on hypersonic flow and using steam-hydrocarbon reforming yields, and plasma setup acting on the airflow aerodynamic performance. A schematic of the Ajax concept HFV is shown in Fig. 1. The first two technologies are discussed next.

Received 30 January 2007; revision received 26 March 2008; accepted for publication 6 July 2008.

*Professor, Head of Hypersonic Technologies Department, St. Petersburg State Polytechnic University; Director General and Chief Designer, Hypersonic Systems Research Institute.

†Senior Research Scientist, Head of Thermal Chemistry Department, Hypersonic Systems Research Institute.

II. Active Thermal Protection and Fuel Conversion

Active thermal protection system is one of the energy-transfer channels [4,5]. It represents an aggregate of recuperative heat exchangers placed in the most heat-stressed parts of the airframe and engine structures, wherein various physical and chemical processes occur, ranging from elementary heating of coolants to endothermic catalytic reactions. One of the coolants and a reagent is a hydrocarbon fuel (aviation kerosene), and an energy source for realization of physical and chemical transformation is used heat from aerodynamic heating and from a power plant. Thus, from the energetic point of view, Ajax-conception vehicles use onboard primary energy (in the form of fuel chemical energy) more efficiently than other structures. The thermal protection system under consideration fulfills not only traditional function, providing for normal temperature conditions of the vehicle structure, but serves as a preparation system for the new modified fuel comprising molecular hydrogen. It became possible due to chemical-heat regeneration.

A. Chemical-Heat-Regeneration Technique

Analysis of operation of various energy installations shows that the efficiency of organic fuels used by them remains rather low: not exceeding 40%. It can be explained by the fact that fuel energy transformation in the existing thermal power plants is accompanied by considerable heat losses into the environment through apparatus walls with exhaust gases, as well as by means of irreversible losses in the process of fuel combustion itself. The preceding losses could be avoided to a considerable degree through their use in special catalytic reactors and heat exchangers by transforming initial organic fuel into a new fuel: the so-called synthesis gas ($H_2 + CO$).

Thermodynamic analysis of the initial and converted fuel-combustion processes indicates that the amount of irreversible losses in the last case is lower too. Thus, chemical heat use and converted fuel combustion result in the efficiency enhancement of energy installations as well as in fuel savings. Moreover, when burning synthesis gas, harmful emissions into the atmosphere are lower. In the installations with chemical-heat regeneration, the process of fuel energy transformation is divided into two stages. The first stage consists of heat pickup from a heated surface and conducting the endothermic reaction of the initial fuel conversion. The second stage consists of the reaction and yields combustion (i.e., combustion of the converted fuel with higher calorific power than with the initial reagents). The first stage is quite noteworthy as a cooling technique (thermal protection) for heat-stressed structures. Thermal protection

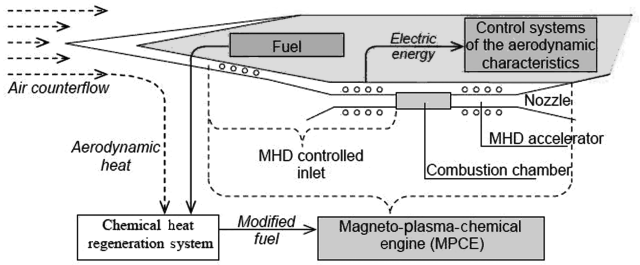

Fig. 1 Schematic diagram of the Ajax concept HFV.

is accomplished not only at the expense of heat removal by means of convection and radiation, but through its absorption at the phase and chemical transformations, whereas the latter are not of a destructive character (as is the case with ablative thermal protective materials) and serve as a means of new fuel production.

The development of thermochemical methods to improve efficiency of the fuels used with concurrent use of heat losses necessitates the solution of a number of scientific and applied problems, including selection of fuels and endothermic processes; development of catalysts for realization of chemical reactions; manufacture of heat-exchanging equipment, particularly thermochemical reactors (TCRs) as structural components of thermal protection and the fuel-transformation system; organization of the combustion process; and selection of the combustor design for the modified fuel.

B. Steam Reforming

Among the multitude of existing endothermic reactions [6] we first consider steam-hydrocarbon reforming. The selection in its favor has been made on a number of criteria, particularly on the amount of hydrogen produced and the value of mean molecular mass of the reaction yields, heat of reaction, temperature level and velocity, amount of used heat flux, and others.

The heat of a reaction has a pronounced effect on the amount of heat absorbed in the thermochemical reactor. Let us consider, as an example, the steam-methane-reforming reaction at the following component stoichiometric ratio (0.47 kg CH_4 and 0.53 kg H_2O):

$$CH_4 + H_2O = 3H_2 + CO - 207 \text{ kJ}$$

Enthalpy change of the original reaction components at the preparation stage (the so-called physical cooling resource) is a result of the processes of heating, vaporization, and overheating of the water-methane mixture; in the range from $T = 273$ to 1000 K, it makes a $\Delta H_{\text{phys}} = 3.3$ MJ/kg mixture. The chemical-cooling resource, equal to the heat of a reaction, makes a $\Delta H_{\text{chem}} \sim 6.6$ MJ/kg mixture. Thus, the complete cooling resource is a

$$\Delta H_{\Sigma} = \Delta H_{\text{phys}} + \Delta H_{\text{chem}} = 9.9 \text{ MJ/kg}$$

mixture. For comparison purposes, the enthalpy variation of liquid hydrogen heated to self-ignition temperature ($\Delta T = 830$ K) is $\Delta H_{\text{phys}} = 12$ MJ/kg. Thus, as to the available cooling resource, a hydrocarbon and water composition subjected to the preceding chemical transformation is approaching the version of liquid hydrogen cooling.

Application of water in steam-hydrocarbon reforming results in the reducing of the heat of combustion for the converted fuel, compared with the initial fuel. It is supposed, though, that the bulk of the initial hydrocarbon (no less than 80%) is supplied directly to the combustor. The converted fuel, mixing with the initial fuel, acts as a hydrogen source (needed to initiate supersonic combustion in the scramjet). It should be noted that catalytic steam-hydrocarbon conversion (its thermal effect and hydrogen amount produced) surpasses by several times the noncatalytic endothermic processes such as pyrolysis, cracking, and depolymerization of hydrocarbons. The problem lies in the creation of the extended catalytic surface of heat exchange and maintenance of its properties throughout the entire period of product operation.

A specific type of hydrocarbon-steam-conversion reaction depends on the process conditions (temperature, pressure, hydrocarbon-water ratio, and so on). For example, at high temperatures ($T > 1200$ K), the reactions proceed practically until the formation of only H_2 and CO (high-temperature conversion):

$$aC_nH_m + bH_2O \rightarrow fH_2 + gCO \tag{1}$$

At low temperatures ($T < 700$ K), product output is shifted considerably toward the formation of CH_4 and CO_2, and the resulting reaction of gasification can be presented as follows (low-temperature conversion):

$$aC_nH_m + bH_2O \rightarrow dCH_4 + eCO_2 \tag{2}$$

As a general case, both reactions (1) and (2) are accompanied by two more independent reversible reactions that determine the equilibrium composition of the converted gas:

$$CH_4 + H_2O \leftrightarrow CO + 3H_2 \tag{3}$$

$$CO + H_2O \leftrightarrow CO_2 + H_2 \tag{4}$$

Unfortunately, the process of hydrocarbon decomposition is complicated by undesirable reactions of free carbon (coke) formation. Two-stage steam conversion of liquid hydrocarbons (Fig. 2) is one of the ways to decrease coke formation in the components of the thermal protection system. During the first stage, liquid hydrocarbons are gasified under low temperature ($T = 550$–700 K) through reaction (2). At the second stage, gasification products are transformed according to reactions (3) and (4) under $T = 1000$–1200 K. Such process organization has some advantages over the one-stage scheme. It is not vapors of liquid hydrocarbons that undergo high-temperature conversion, but a gaseous mixture consisting of methane (resistant to coke formation) and carbon dioxide.

Presented in Fig. 2 is a scheme as the two-stage process becomes simplified, turning into one stage if 1) methane is the original fuel and 2) the duration of the setup operation is not too long, allowing the coke-formation process to be neglected: a fact proven by experiments [7]. It is expedient in both cases to immediately conduct the high-temperature steam reforming.

The elaboration of a new chemical-heat-regeneration technology, as applied to heat engines of various designations, calls for a new

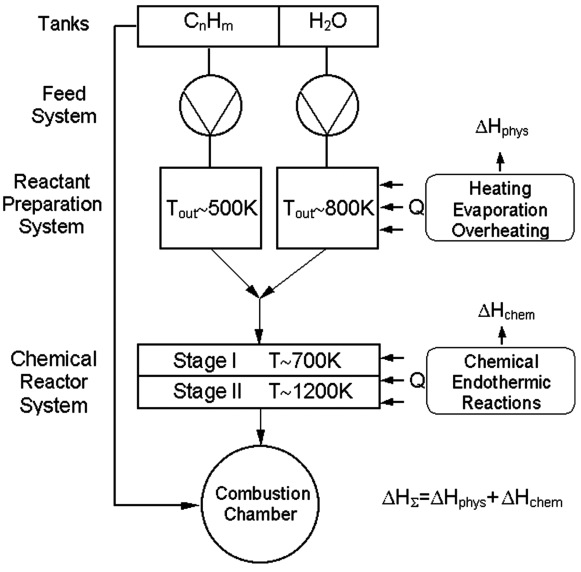

Fig. 2 Schematic diagram of fuel transformation onboard the HFV using steam-hydrocarbon reforming.

approach to production of both catalysts and conversion units in general. Onboard catalysts, apart from traditional requirements to their activity, selectivity, and durability, have to meet a number of specific requirements such as being a single whole with a heat-transferring surface; possessing high thermal conductivity, thermocyclic strength, chemical heat resistance, and resistance to impact loads and vibrations; working under the action of heat fluxes; being large in magnitude, and being variable in time. These requirements are met by a number of catalysts under development at present, particularly catalytic coatings (planar catalysts) directly deposited on the heated wall. Thermal resistance and catalytic coat activity issues have been considered at some length in [8]. It was shown that the most efficient coatings have the following parameters: width of 0.01 mm, pore diameter of less than 3×10^{-5} mm, and thermal conduction $\lambda \geq 1$ W/(mK).

C. Experimental Investigation

To study the process of hydrocarbon fuel transformation, TCRs of various configurations have been used. One of the TCR fragments is shown in Fig. 3. The reactor itself represents a cavity formed by two coaxial cylinders with 500 mm length and clearance width $d =$ 2.0 mm between them. The inner surface of this cavity was coated with a Ni–Cr catalyst, and methane was to act as one of the reagents. A schematic of the setup for methane reforming is presented in Fig. 4. The water was heated and evaporated in a water evaporator (1). Heating of the steam and methane from the cylinder was done in electric heaters (2 and 3, respectively). Then came the blending of reagents and their supply at ~550°C to the TCR (4), in which the chemical endothermic reaction proceeded. Heat input to the steam-methane mixture was realized through the inner wall of the reactor. The high-temperature nitrogen jet from the plasmatron (5) served as a heating source. The TCR inner-wall temperature was taken by thermocouples (6). Samples for analysis of the reaction-yields composition were taken with the help of samplers (7).

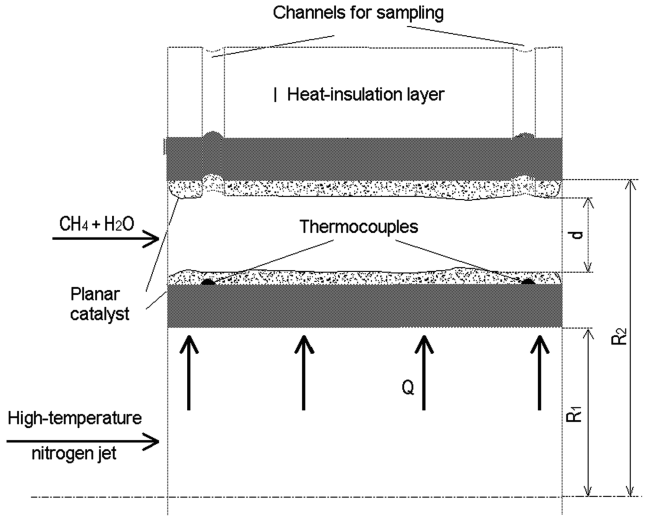

Fig. 3 Fragment of the cylindrical TCR (not to scale).

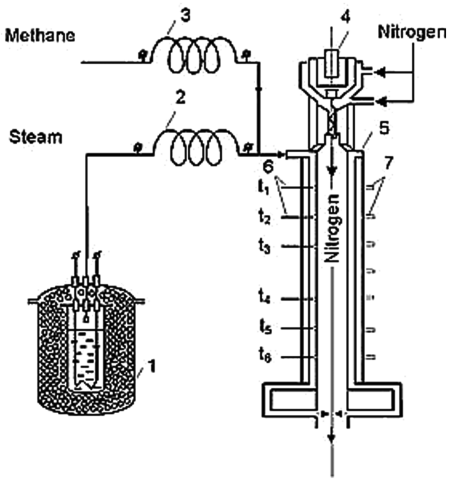

Fig. 4 Schematic diagram of setup for steam-methane reforming.

Figure 5 shows a typical profile of the reactor's wall-temperature distribution. The initial part of the curve corresponds basically to the mixture's convective warmup to the temperature of reaction. Then gradual deceleration of wall-temperature increase starts, followed by its drop caused by intensive heat extraction for endothermic reaction of steam reforming. When feeding neutral-gas nitrogen to the reactor, this phenomenon is not observed: convective warmup of the mixture (dotted line) lengthwise of the reactor occurs instead.

Figure 6 shows distributions of methane and hydrogen concentrations lengthwise of the reactor that bear witness to the chemical reaction inside the reactor. Figures 7 and 8 present dependencies of methane conversion degree X and average density of heat flux lengthwise of the reactor q_{av} on the vapor-methane mixture velocity at the reactor inlet. Some conclusions can be drawn from their analysis:

1) The conversion degree increases with velocity decrease, which can be explained by the increase of residence time of the reacting substance.

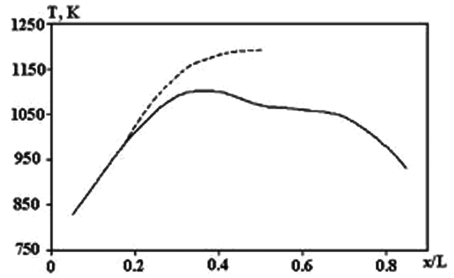

Fig. 5 Temperature distribution on the TCR wall.

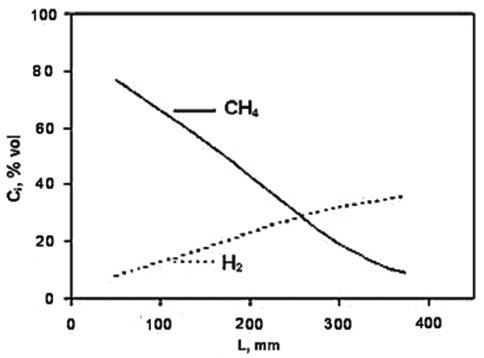

Fig. 6 Distribution of methane and hydrogen concentrations lengthwise of the TCR.

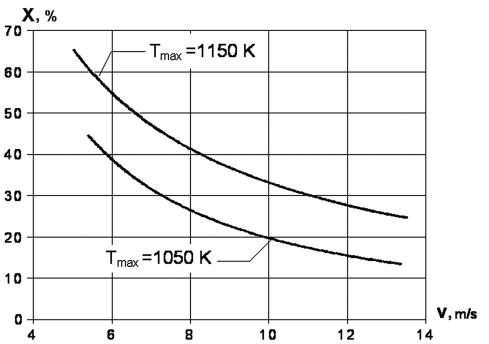

Fig. 7 Methane conversion degree.

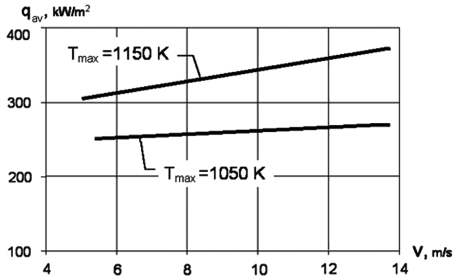

Fig. 8 Average heat-flux density.

2) The average density of the heat flux increases with velocity increase. This effect is associated with the redistribution of contributions made by chemical and convective components of the heat flux being absorbed.

3) The wall-temperature increase at the fixed ratio H_2O/CH_4 has a favorable effect on the degree of conversion value and on the absorbed-heat-flux value.

4) To get the maximum heat absorption and molecular hydrogen production, it is necessary to have the system of various TCRs (size, catalyst type, and operational parameters) optimal as to their target functions.

Summarizing the application results of steam-methane reforming under standard (industrial) conditions and laboratory investigation of the process at the unlimited heat supply, one can draw a conclusion on the possibility of thermochemical transformation of the primary fuel in the system of reactors with various degrees of conversion (10–100%) of the heat use in a wide range of heat loads (0.05–1 MW/m^2).

III. Use of the MHD Systems for Scramjet Performance Control

Nowadays, the supersonic combustion ramjet (scramjet) is recognized as the most promising engine for mastering hypersonic flight velocities. With a scramjet, a vehicle surface is used [9] for preliminary compression of the freestream. But complicated flow structure in its channel increases the probability of flow separation and hampers efficient fuel burning in the combustor [10]. At a flight velocity below that designed for the scramjet, inlet airflow rate and compression ratio are decreased. In addition, any flight-velocity variation results in significant reshaping of the flow structure in the engine, thus making its operation efficient only over a limited velocity range. Because of the preceding, a set of challenges is currently under investigation that is associated with the development within the framework of the Ajax concept [2] of a new engine, the so-called ramjet with MHD interaction, and MPCE in our nomenclature. The use of volume MHD interaction in the scramjet duct allows creation of the controllable inlet, optimization of airflow parameters, ensuring of the scramjet operability, and production of electric power in a wide range of hypersonic velocities [11–18].

A. Elaboration of the MHD System Application Concept for Airflow Deceleration and Compression

To expand the scramjet operational range, an additional mechanism of action upon the flow is needed that would provide for the extra deceleration and compression of the flow within the inlet. Presented in the Fig. 9 simplified MPCE schematic is the gist of the scramjet [19], complete with MHD systems in its duct. In the external section of the inlet, compression of free airflow is realized in the system N of the shock waves and its total θ_N turn and in the internal part of the inlet-flow θ_N turnaround and its supplementary compression. An ionizer is used to ensure the required flow conductivity when natural conductivity does not provide for the necessary degree of MHD interaction.

The external MHD generator is used for the flow profile control, the adjustment of the airflow rate within the MPCE duct, and the pressure increase. The internal MHD generator is used for pressure increase and prevention of flow separation. Electric power produced

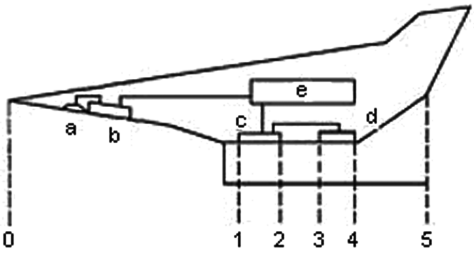

Fig. 9 MPCE schematic: air inlet (0–1), internal MHD generator (1–2 and c), combustor (2–3), MHD accelerator (3–4 and d), nozzle (4–5), ionizer (a), external MHD generator (b), and onboard systems (e).

by the MHD generators is spent for the needs of the ionizer, onboard equipment, and extra acceleration of combustion yields in the MHD accelerator. For a mathematical description of the MHD system volumetric action on the flow, we select a quasi-one-dimensional approximation with non-(heat)-conductive nonviscous ideal gas with a constant heat capacity [11,20,21]. It is anticipated that a pressure gradient in the MHD channel is proportional to the force acting on the flow from the magnetic field side:

$$\frac{\mathrm{d}p}{\mathrm{d}x} = \xi(x)(1-k)^2\sigma B^2 v \tag{5}$$

where p is static pressure in the flow, v is the flow velocity, x is the longitudinal x coordinate, σ is flow conductivity, B is magnetic induction, and $\xi(x)$ is the coefficient of proportionality. All theories concerning the MHD process presented in this work ignore the phenomenon of electron slip. The class of Eq. (5) solutions with condition $\xi = \text{const}$ conforms to a number of important flow cases in the MHD channel under consideration. Examination of the flow in a Hall MHD channel leads to an analogical condition. Such a condition allows the finding of simple analytical expressions for the flow parameters at the MHD channel outlet [20,21]. If we mark the values of flow parameters at the MHD channel inlet by index 1 and those at the outlet by index 2, then the variation of flow parameters in the MHD duct will be described by the following relations:

$$\begin{aligned} \frac{T_2}{T_1} &= 1 + \frac{1-k}{k}\left(1 + \frac{\gamma-1}{2}M_1^2\right)(1+\xi)\eta, \\ \frac{v_2}{v_1} &= \sqrt{1 - \frac{1+\xi\,(1-k)}{k}G\eta} \end{aligned} \tag{6}$$

$$\frac{p_2}{p_1} = \left(\frac{T_2}{T_1}\right)^{\frac{\gamma}{\gamma-1}\frac{\xi}{\xi+1}} \tag{7}$$

where the multiplier takes the form

$$G = \frac{2 + (\gamma-1)M_1^2}{(\gamma-1)M_1^2}$$

T is the temperature; M is the Mach number; γ is the adiabatic exponent; η is the enthalpy extraction into electric energy; and condition $\xi = \text{const}$ includes, as a particular case, frequently considered flow conditions featuring one of the flow parameter's conservation [20,21]. Table 1 presents the values of the ξ parameter corresponding to these regimes.

Expressions (5–7) allow description of a MPCE scheme operation in one-dimensional approximation. At this stage, we shall restrict ourselves to considering a case when flow conductivity is provided for without using an ionizer. Let us assume that the inlet has the following characteristics: N is the number of shocks in the external part, θ_N is the flow total turning angle, Γ_{in} is the coefficient of total pressure recovery in the inlet. Coefficient of total pressure recovery characterizes losses of total pressure of the air mass supplied to the engine. It is defined as the ratio of the mean total pressure of the stagnated flow in the measuring duct at the engine entrance to the total pressure in the free flow.

Table 1 Parmeter ξ values for some flow conditions in the MHD generator of the Faraday type

Flow conditions	Parameter ξ value
$\rho = \text{const}$	$\gamma - 1$
$p = \text{const}$	0
$T = \text{const}$	-1
$M = \text{const}$	$-\{1 + [2/(1-k)(\gamma-1)M_1^2]\}(1/G)$
$v = \text{const}$	$-1/(1-k)$

Then temperature T, velocity v, and pressure p at the intake and outlet are connected by the relations

$$\frac{p_1}{p_0} = \Gamma_{\text{in}}\left(\frac{T_1}{T_0}\right)^{\frac{\gamma}{\gamma-1}}, \qquad \frac{v_0^2}{2} + c_p T_0 = \frac{v_1^2}{2} + c_p T_1 \tag{8}$$

where c_p is the specific thermal capacity of the air at constant pressure.

The MHD generator is characterized by parameter ξ_1, load factor k_1, and enthalpy extraction ratio η. Flow parameter variation in the MHD generator channel is defined by the following expressions:

$$\begin{aligned} \frac{p_2}{p_1} &= \left(\frac{T_2}{T_1}\right)^{\frac{\gamma}{\gamma-1}\frac{\xi_1}{\xi_1+1}}, \\ \frac{T_2}{T_1} &= 1 + \frac{1-k_1}{k_1}\left(1 + \frac{\gamma-1}{2}M_1^2\right)(1+\xi_1)\eta \end{aligned} \tag{9}$$

Combustor operation can be viewed as being under constant pressure conditions. In addition, it is worth noting that fuel mass flow rate is usually much less than air mass flow rate. As such, heat release in the combustor can be considered without a supply of extra mass. A temperature ΔT rise in the combustor is determined by the ratio [9]

$$\Delta T = \frac{H_u}{c_p(KL_0 + 1)} \tag{10}$$

where H_u is the fuel heating capacity, L_0 is the stoichiometric coefficient, and K is the excess-air coefficient.

The MHD accelerator is characterized by parameters ξ_3 and k_3. At this stage, it is also assumed that all of the power produced by the MHD generator is transferred to the MHD accelerator. Lower indices correspond to the subsystem's arrangement in the MPCE channel (Fig. 9). Parameter variation in the MHD accelerator channel is described by expressions analogous to ratio (9). As for the nozzle, it is believed that the flow therein is isentropic and the outlet pressure is equal to the surrounding medium ($p_5 = p_0$). Taking that into consideration, for flow temperature at the nozzle section, we obtain [11,22]

$$T_5 = T_4 \Bigg/ \left(\Gamma_{\text{in}}^{(1-1/\gamma)}\left[\frac{T_1}{T_0}\left(\frac{T_2}{T_1}\right)^{\frac{\xi_1}{\xi_1+1}}\left(\frac{T_4}{T_2+\Delta T}\right)^{\frac{\xi_3}{\xi_3+1}}\right]\right) \tag{11}$$

where values T_1 and Γ_{in} are determined on the basis of numerical computation of the flowfield for the selected inlet configuration. In this paper, flowfield computation was performed in two-dimensional Euler approximation.

The obtained temperature T_5 value allows determination of the velocity for gas outflow from the nozzle using the energy-conservation law:

$$v_5 = \sqrt{v_0^2 + 2c_p(T_0 + \Delta T - T_5)} \tag{12}$$

Neglecting the fuel flow rate s compared with the airflow rate, we obtain the expression for the MPCE specific impulse [23]:

$$I_{\text{sp}} = \frac{KL_0}{g}(\varphi v_3 - v_0) \tag{13}$$

where g is the acceleration of gravity, and φ is the nozzle nonideality factor.

Equations (6–13) allow calculation of the MPCE specific impulse at the prearranged parameters of the inlet, MHD systems, and combustion chamber. The specific impulse turns out to be a function of many parameters: $K, L_0, M_0, T_1, \Gamma_{\text{in}}, K_1, \xi_1, \eta_1, \Phi, k_3, \xi_3$. T_1, and Γ_{in} values were being determined through inlet parameters N and θ_N using a computation technique analogical to that presented in [24], with subsequent averaging of the outlet-section parameters of the air inlet.

To determine the variation range for the parameters of MPCE subsystems in which MHD system usage allows an increase of the propulsion specific impulse, it is possible to obtain the following inequality:

$$\xi_1 > \frac{T_1}{\Delta T}\frac{1 - k_1/k_3}{1 - k_1} \tag{14}$$

Because the load factor of the MHD generator meets condition $0 < k_1 < 1$ and the load factor of the MHD accelerator meets condition $k_3 > 1$, then the MPCE specific-impulse increase in the configuration at hand occurs at ξ_1 positive values. According to Eq. (5), it corresponds to the MHD generator operating under conditions with a pressure increase lengthwise of the channel. It is evident that the requirements for the pressure gradient value sink to a lower level with ΔT increase and T_1 decrease. Figure 10 presents dependencies of the MPCE specific impulse on the ratio η for ideal and nonideal gas. The $\eta = 0$ value corresponds to a scramjet. The MPCE specific impulse here is normalized to the specific impulse of a scramjet.

Specific-impulse dependence on the MHD generator load factor for $M = 6$ hypersonic flow (Fig. 11) has a distinct maximum corresponding to MPCE, with the inlet characterized by a minimal value of the total turning angle of the flow ($\theta_N = 0.2$ rad). It is established that in all MHD versions considered, energy conversion in a propulsion channel results in a specific-impulse increase, with a more significant positive effect for the nonideal nozzle.

B. Concept of the MHD Generator for Mass Flow Rate and Flow Structure Control

In this chapter, the possibility of using volume flow deceleration by magnetic field is studied in an effort to produce a variable-geometry air inlet that could operate in a wide velocity range. The

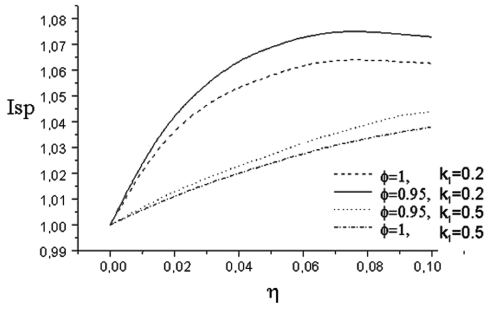

Fig. 10 Dependence of the specific impulse on the enthalpy extraction ratio for various values of the parameter φ.

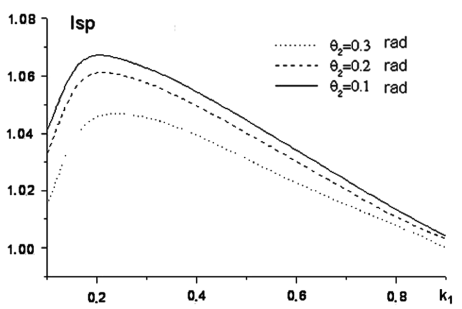

Fig. 11 Dependence of the specific impulse on the load for various values of parameter θ_N: $M = 6$, $\eta = 0.1$, $\xi_1 = 1$, $k_1 = 0.2$, and $k_3 = 1.2$.

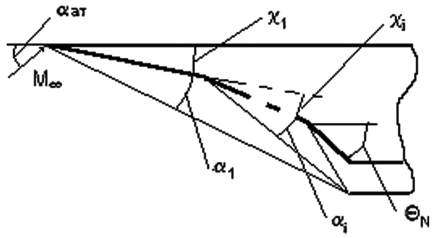

Fig. 12 Scramjet inlet geometry diagram.

MPCE input device under investigation contains a planar multishock inlet of external compression and an internal compression duct in the MPCE generator channel [25,26]. The general design diagram of the inlet is presented in Fig. 12. Here, M_∞ is the Mach number of the oncoming flow. The inlet geometry is defined by the following parameters: flow total turning angle θ_N, number of shocks N, design angle of attack α_{at}, design Mach number M_d, and wedge angular value x_i, where i is the shock number ($i = 1, \ldots, N$).

Under design conditions flight, all shocks are focused on the leading edge of the inlet entrance slit. At the external air inlet, the flow turns through the $\theta_N + \alpha_{\text{at}}$ angle. The wedge angular value is determined from the shock equal intensity condition. Their sum meets ratio $x_1 + \cdots + x_N = \theta_N$. Under offdesign conditions flight, the shocks equal intensity condition is not complied with. At the air inlet throat, flow turnaround in the system of oblique shocks occurs.

To describe the flow parameters in the MHD duct of the controllable air inlet, two-dimensional Euler approximation was used. Steady-state flow conditions described by following equations have been considered:

$$\frac{\partial \rho v_x}{\partial x} + \frac{\partial \rho v_y}{\partial y} = 0 \qquad \frac{\partial (h_e + p) v_x}{\partial x} + \frac{\partial \rho v_y}{\partial y} = q_g + q_r \tag{15a}$$

$$\frac{\partial (\rho v_x^2 + p)}{\partial x} + \frac{\partial \rho v_x v_y}{\partial y} = f_x \qquad \frac{\partial (\rho v_y^2 + p)}{\partial y} + \frac{\partial \rho v_x v_y}{\partial x} = f_y \tag{15b}$$

where $h_e = \rho[c_v T + (v_x^2 + v_y^2)/2]$ represents the total specific thermal and kinetic flow energy, value $p = R_{rp} T / m_0$ represents gas static pressure, q_g is the volume density of thermal output produced by the MHD generator, q_r is the volume density of thermal output released by ionizer, ρ is the flow density, R_r is the universal gas constant, and m_0 is the gas molecular mass.

The quantity

$$\mathbf{f} = \{f_x, f_y, 0\} = [\mathbf{j} \times \mathbf{B}] \tag{16}$$

is the volume density of the Lorentz forces, and the quantity

$$q_g = \mathbf{jE} \tag{17}$$

is the power density of the MHD generator.

The density vector of induced current in the last two expressions is given by the component $\mathbf{j} = \{0, 0, j_z\}$. It is connected with the magnetic induction vector $\mathbf{B} = \{B_x, B_y, 0\}$ and induced electric field vector $\mathbf{E}$ by the generalized Ohm law:

$$\mathbf{j} = \sigma(\mathbf{E} + [\mathbf{v} \times \mathbf{B}]) \tag{18}$$

where σ is flow conductivity. It depends on the power q_i deposited to ionize the flow volume unit as well as on coordinates x and y. Through the application of the results set forth in [27], computation of the preceding value has been performed. The value q_r is the thermal capacity released in a volume unit due to the charged particle recombination processes. When the velocity of these processes is sufficiently high, it can be taken approximately that $q_r = q_i$.

Numerical computations of density fields in the MHD-controlled inlet of a MPCE have been conducted in a wide range of geometrical parameter variations of the free flow, ionizer, and MHD systems.

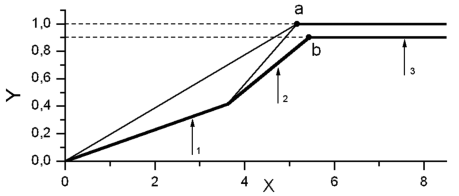

Fig. 13 Scramjet inlet geometry with $\theta_N = 15$ deg and $M_d = 10$.

One of the cases under consideration corresponds to the air inlet with the geometry shown in Fig. 13 on the x–y coordinates. Here, F_{th} is an inlet throat parameter:

$$F_{\text{th}} = (Y_a - Y_b)/Y_a \tag{19}$$

The typical locations of external and internal MHD generators when considering various versions of the MPCE system integration are marked by arrowheads.

Figure 14a shows computed flow density contours at the inlet without MHD control under design conditions $M_\infty = M_d = 10$. Figure 14b shows flow density contours at the inlet without MHD control under offdesign conditions and $M_\infty = 12$. Figure 14c shows flow density contours at $M_\infty = 12$ with MHD interaction

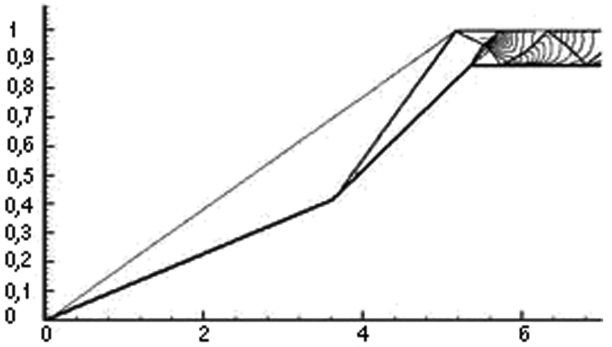

a) M_∞=M_d=10, B=0

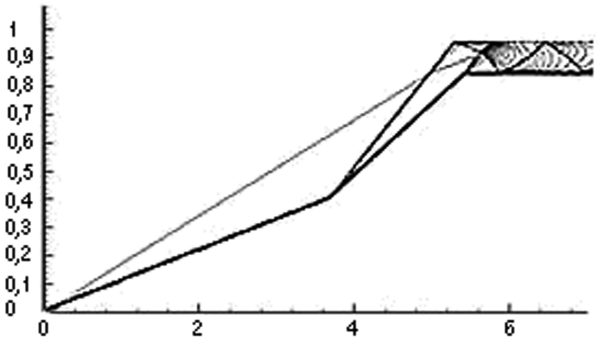

b) M_∞=12, B=0

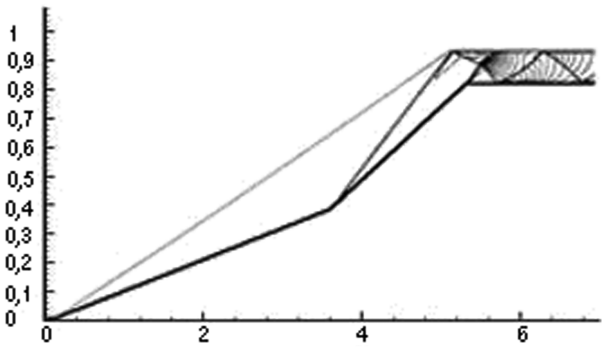

c) M_∞=12, B=5.3 T

Fig. 14 Density contours in the MHD-controlled air inlet at $M_\infty \geq M_d$.

($B = 5.3$ T). It is evident that the flowfield under offdesign conditions with MHD interaction has an appearance similar to the flowfield under design conditions. Analogical results have been obtained by the other authors [28,29].

Figure 15 illustrates the possibilities for flowfield control within an air inlet through the external MHD generator under conditions when the Mach number is below its design counterpart. In this case, MHD interaction allows mass airflow rate increase; here, $M_\infty = 6$ (i.e., distinctly less than its design value). Figure 15a depicts flowfield density contours in the air inlet without MHD control. Figure 15b shows flowfield density contours in the air inlet with MHD control. The ionization zone in these cases constitutes the infinite layer limited by the condition $x_i < x < x_i + \Delta x$. Figure 15b shows the flowfield in the MHD-controlled inlet for a case in which the magnetic induction field has but one y component and ionization zone presents a narrow stripe.

Figures 16–19 show the results of another series of computations in two-dimensional Euler approximation of the flow in the duct of the MHD-controllable inlet. Parameter transverse distribution in the MPCE-assigned section upstream of the combustion chamber is shown there.

Thus, in Figs. 16 and 17, parameter comparison in the scramjet inlet (magnetic field is unavailable) and within the MPCE is given at the preset magnetic field distribution for two possible versions of ionization-zone assignment: 1) homogeneous ionization over all space and 2) in a selected ionization zone allowing investigation of the inhomogeneity factor for ionization sources.

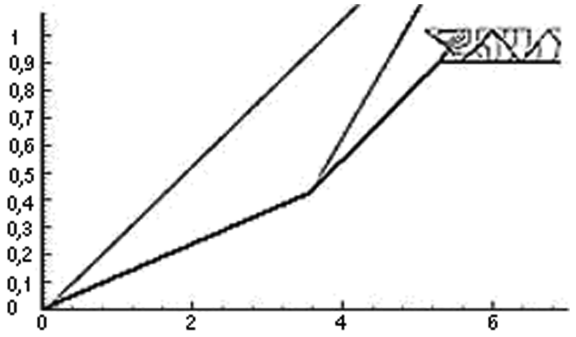

a) M_∞**=6,** B**=0**

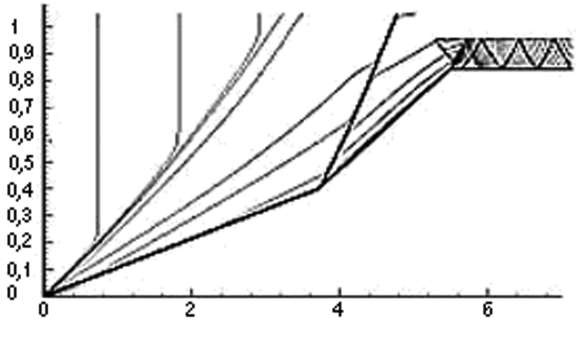

b) M_∞**=6,** B**=3Tπ,** $|B_x/B_y|$**=0,** q_i**=10^{-2} W/cm^3,** x_i**=0,** Δx**=5**

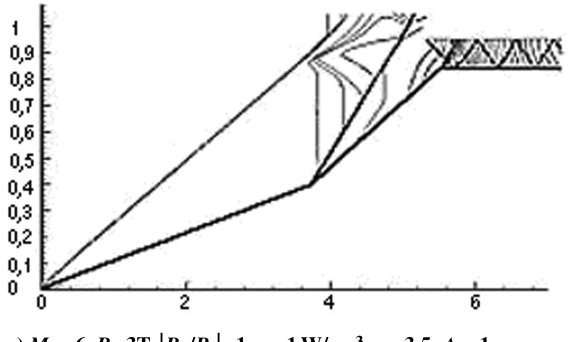

c) M_∞**=6,** B**=3T,** $|B_x/B_y|$**=1,** q_i**=1 W/cm^3,** x_i**=3.5,** Δx**=1**

Fig. 15 Density contours in the MHD-controlled air inlet at $M_\infty < M_d$**.**

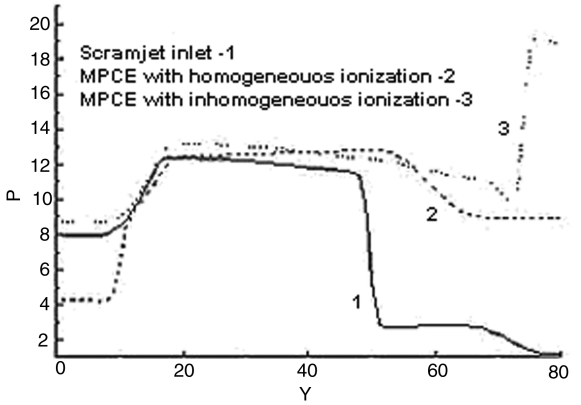

Fig. 16 Pressure distribution in the inlet transverse section at a preset magnetic field distribution; parameter values are presented accordingly in Fig. 14.

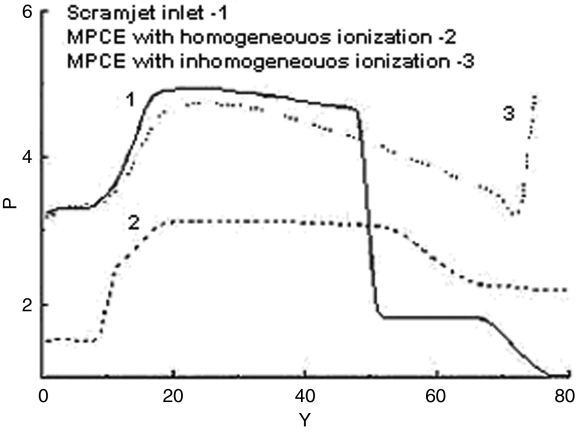

Fig. 17 Density distribution in the inlet transverse section at a preset magnetic field distribution; parameter values are presented accordingly in Fig. 15.

It can be seen from the figures provided that usage of the MHD systems in the inlet duct allows pressure increase, and special selection of the ionization zone (inhomogeneous ionization) allows an increase of both pressure and flow density. Thus, the investigations conducted have shown that the MHD-controlled inlet with inhomogeneous flow ionization is a more efficient system than the one with homogeneous ionization.

In principle, it is possible to realize flow control within the MHD duct through MHD generator load variation. Other crucial possibilities of flow control are achieved at the expense of a configuration change of the ionized formation (as in the preceding case of inhomogeneous ionization), change of field configuration, and variation of flow conductivity.

As a result of load variation, the magnitude of the transverse induced electric field E is changed. This parameter characterizes dependencies presented in the figures. The obtained results show that the control technique for inlet parameters through variation of system electric parameters allows significant variation of pressure and density distribution at the entrance to the combustor (Figs. 16 and 17). Thus, realization of the MHD impact on the stream considerably changes the flowfield. In particular, from computational results, it follows that the MHD interaction leads to a flow density increase and makes the density transverse distribution more uniform.

We have been also concerned with the investigation of MHD system parameter impact upon the velocity of the mass flow rate. Figure 18 shows the dependencies of the relative velocity of the mass flow rate on the power density spent for the flow realization at its different stations: here, ϕ is the mass airflow rate with MHD interaction and ϕ_0 is without MHD interaction.

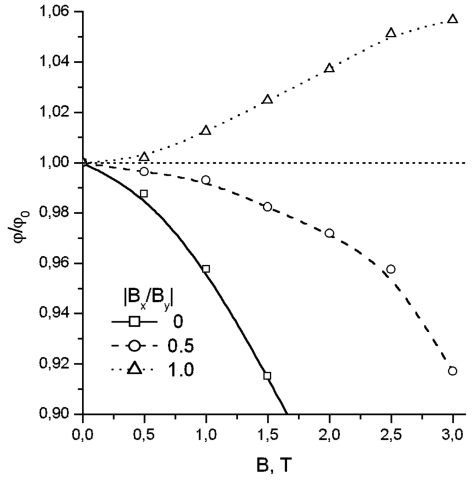

Fig. 18 Dependence of mass flow on magnetic induction at the following MPCE parameters: $M_\infty = 6$, $q_i = 10^{-2}$ W/cm^3, $x_i = 0$, and $\Delta_x = 5$.

Figure 19 provides dependencies of the relative mass airflow rate on the power density spent for ionization at different arrangements of ionization sources. It can be seen that the configuration, magnetic field magnitude, location of ionization zone, and amount of power density spent on ionization have a significant effect on the mass airflow rate. The investigation results allow one to draw a conclusion that at $M_\infty < M_d$, the result of the MHD interaction depends on many parameters, whereas a MHD interaction increase can lead to an increase as well as a decrease of the mass airflow rate.

Table 2 presents the correlation between some MPCE and scramjet performances at offdesign flight conditions for $M_\infty = 6$ and 8 when $M_d = 10$. Here, M_∞ is the Mach number of the free flow, ϕ is the mass airflow rate, and R_T is engine thrust, which is calculated from the mass airflow rate and specific impulse:

$$R_T = \phi I_{\text{sp}} \tag{20}$$

The results are presented for the ratio of calculated MPCE characteristics to the appropriate scramjet characteristics without MHD control. The value q_i equal to the specific density spent for ionization is given in the form of the relation to some typical parameter q_{cr}, which will be discussed in detail in the subsequent paragraphs. It is evident that the MHD interaction upon the flow allows considerable enhancement of the mass airflow rate (up to

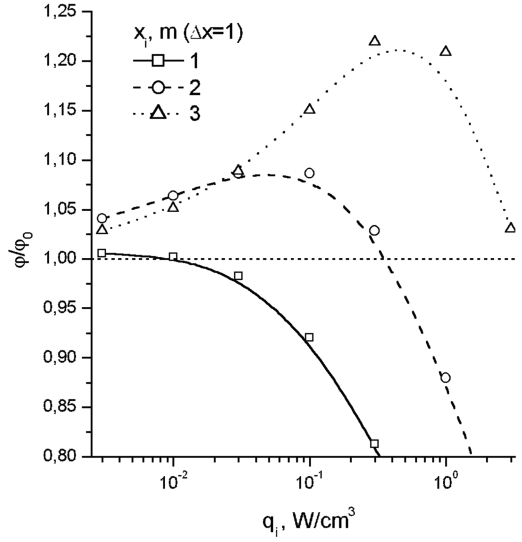

Fig. 19 Dependence of mass flow on the amount of energy deposition spent for flow ionization at the following MPCE parameters: $M_\infty = 6$, $B = 3$ T, and $|B_x/B_y| = 1$.

Table 2 Correlation between some MPCE and scramjet characteristics

M_∞	q_i/q_{cr}	ϕ/ϕ_0	I^*_{sp}/I_0	R^*_m/R_{0m}
6	0.05	1.25	1.12	1.40
	0.25	1.32	1.12	1.48
	1.0	1.37	1.10	1.50
8	0.02	1.18	1.02	1.20
	0.08	1.20	1.01	1.21
	0.16	1.23	0.99	1.22

37%) and thrust (up to 50%) at the free flow Mach number $M_\infty = 6$. At $M_\infty = 8$, the MHD interaction effect on propulsion performance is not so significant, and the maximum thrust increase is 22%. The maximum increase for the specific impulse at the considered version is 12% at $M_\infty = 6$.

Thus, the volume interaction of the flow with magnetic field makes it possible to produce a controllable air inlet. The farther flight conditions are from the design conditions, the more significant is the effect of the MHD interaction on thrust characteristics [30].

The suggested concept of the MHD generator usage for mass flow rate and flow structure control presents an opportunity for ramjet creation that would be capable of efficient operation in a wide range of hypersonic velocities. Its application could do away with difficult-to-realize mechanical control over engine performance techniques, which can be considered as having fundamental importance, along with other technical solutions substantiated in this paper.

C. Investigation of the MHD Generator Concept on Cold Airflow with Nonequilibrium Ionization

The term *cold airflow* as used herein for the purposes of this investigation implies the flow with a thermal ionization degree that is insufficient for realization of the MHD control principles. The importance of this investigation stems from the fact that in the case of insignificant natural flow conductivity, it is necessary to take measures to increase its ionization degree. The estimates show that such a state of affairs is typical for hypersonic flight conditions: that is, an ionizer is a crucial part of any MHD system.

The energy required for the production of one electron–ion pair shall be called the *cost of ionization* and designated as W_i. Analysis of the known ionization techniques shows that from the energy point of view, an electron beam is the least expensive means for gas ionization [31,32]. According to [33], the price of ionization in this method, with electron energy in a beam exceeding 1 KeV, is $W_i \sim 34$ eV. This value insignificantly exceeds the ionization energy for air molecules. A high-voltage impulse discharge has a larger ionization price of approximately 66 eV for air.

Irrespective of the ionization technique, we shall characterize ionizer operation by power q_i deposited per unit volume. Then the ionization rate in the unitary volume will be defined by

$$J_i = \frac{q_i}{W_i} \tag{21a}$$

For example, at the gas ionization by the electron beam, the value of q_i is defined by the ratio

$$q_i = \frac{j_b}{e} D(E_b)\rho \tag{21b}$$

where j_b is the current density in the beam, $D(E_b)$ is the electron breaking ability, and E_b is the electron energy in a beam.

Ionized gas conductance is determined by an electron concentration that is gauged at the stationary state and preset velocity through the rate of their destruction processes. In the case in which the two-part dissociative recombination (e.g., with positively charged molecular ions) is a prevailing process of electron loss, the steady-state value of electron concentration is specified by

$$n_e = \sqrt{\frac{q_i}{k_{\rm dr} W_i}} \tag{22}$$

where $k_{\rm dr}$ is the two-body electron–ion recombination-rate constant.

As a case in point, Fig. 20 provides the dependence of electron concentration on specific costs for ionization q_i calculated in the event of electron beam usage as a means of ionization [22]. The presented dependence is well approximated by the expression

$$n_e = 1.124 \times 10^{12} \sqrt{q_i},\ \text{cm}^{-3} \tag{23}$$

where q_i is given in W/cm^3. Approximation error here does not exceed 30%.

It follows from Eq. (21) that the flow ionization degree can be presented in the following form:

$$\frac{n_e}{n_0} = \sqrt{\frac{q_i/n_0^2}{k_{\rm dr} W_i}} \tag{24}$$

Computational results of the flow ionization degree depending on the value q_i/n_0^2 are given in Fig. 21. Numerical computation results are well approximated by the following expression:

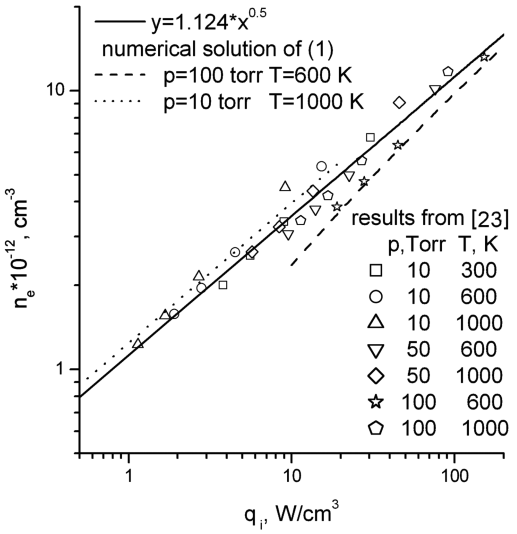

Fig. 20 Dependence of electron concentration in air plasma on energy deposited through an electron beam into the unitary volume in a unit of time.

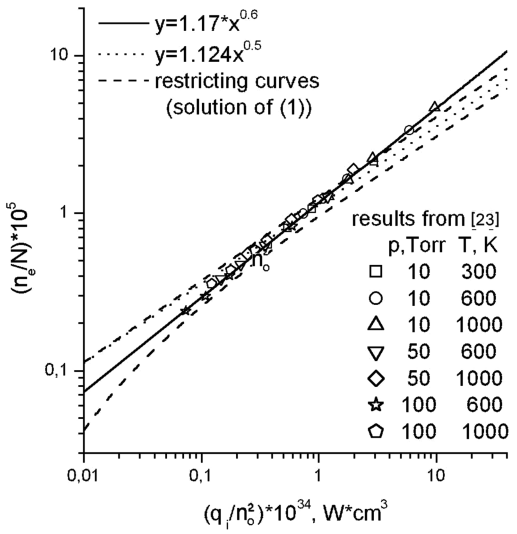

Fig. 21 Dependence of air plasma ionization degree on energy deposited through an electron beam into the unitary volume in a unit of time.

$$\frac{n_e}{n_o} = 1.17 \times 10^{-5} \left(10^{34} \frac{q_i}{n_0^2}\right)^{0.6} \tag{25}$$

where q_i is given in W/cm^3 units, and concentration n_0 is in cm^{-3}. Approximation error in this case does not exceed 9%.

Equations (23) and (25) can be used for prompt evaluation of the plasma ionization degree and electron concentration, as well as for analytical computation in the sphere of parameter values meeting the inequality

$$2 \times 10^{-2} < (q_i/n_0^2) \times 10^{34} < 20 \tag{26}$$

Plasma conductivity is connected with electron concentration by the ratio

$$\sigma = e^2 n_e / m_e n_0 k_c \tag{27}$$

where e is the electron discharge, m_e is the electron mass, and k_c is the electron dissipation-rate constant. The expression is deduced from Eqs. (22) and (27) that bound flow conductivity to the specific power spent for ionization:

$$\sigma = \frac{e^2}{m_e n_0 k_c} \sqrt{\frac{q_i}{k_{\rm dr} W_i}} \tag{28}$$

It is evident that the MHD generator with nonequilibrium conductivity could be realized only in the event when the energy spent for flow ionization to produce the required conductivity level would not exceed the energy produced by the MHD generator. Such operation conditions for the MHD generator with ionizer are called the *self-sustained mode*.

The power produced by the MHD generator depends on flow conductivity, flow gasdynamic parameters, MHD performance, and MHD generator type. Thus, conditions wherein the self-sustained mode could be realized depend on many factors, such as MHD generator arrangement within HFVs, ramjet geometry, flight trajectory, MHD performance, ionizer type, etc. In this paper, the version is examined in which the MHD generator of the ramjet is located upstream of the combustor and the MHD accelerator is placed downstream of the combustion chamber (see Fig. 9).

Let us identify the variation region of MPCE parameters wherein the self-sustained mode for the ionizer and MHD generator exists. To do that, we need to correlate the power spent for ionization with the energy produced by the MHD generator. The volume density of the power produced by the MHD generator is given by the expression

$$q_g = k(1-k)\sigma B^2 v^2 \tag{29}$$

where k is the load factor of the MHD generator, σ is the current conductivity, v is the flow velocity, and B is the magnetic field induction.

Because flow conductivity depends on the power spent for flow ionization, the specific energy produced by the MHD generator is a function of the parameter q_1:

$$q_g = k(1-k)B^2 v^2 \frac{e^2}{m_e n_0 k_c} \sqrt{\frac{q_i}{k_{\rm dr} W_i}} \tag{30}$$

Some results of numerical computation of dependencies of MPCE power characteristics on ionizer parameters and the location points for various parameters of the free airflow are presented in Figs. 22–24.

Dependence of $q_g - q_i$ (parameter difference of power produced and energy deposition into ionization) on parameters q_i and B is provided in Fig. 22. Magnetic induction enhancement at the fixed ionization cost leads to the increase of power produced by the MHD generator and expands the range of the self-sustained mode of the MHD with nonequilibrium conductivity.

Figure 22 allows one to assess net power at the fixed values of ionization energy and magnetic field and to see the extent to which power increases with magnetic field increase.

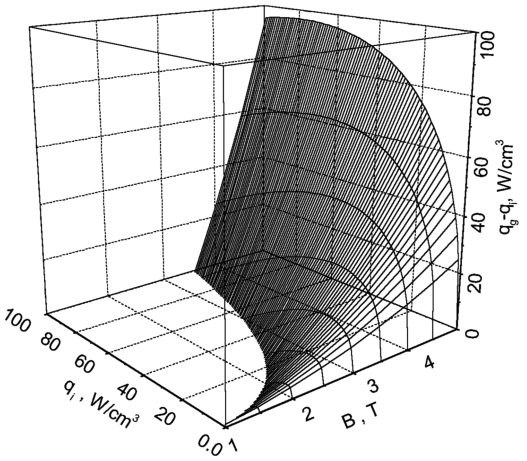

Fig. 22 Power density produced by the MHD generator less the power density spent by the ionizer ($q_g - q_i$), depending on parameters q_i and B; the MHD generator is placed at cross section 2 (Fig. 13); $M_\infty = 6$.

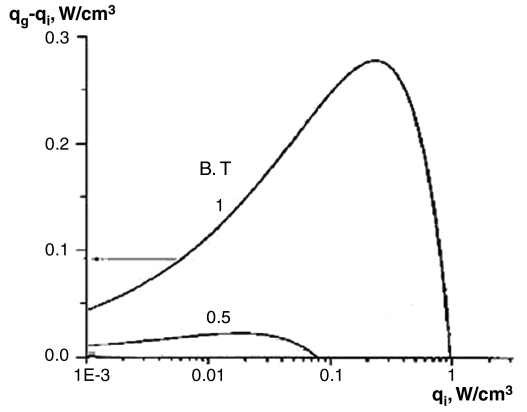

Fig. 23 Power density produced by the MHD generator with nonequilibrium conductivity less flow ionization cost at various values of magnetic induction as a function of the power deposited into ionization; $M_\infty = 6$.

Dependence of $q_g - q_i$ is not monotonic. There exists some optimal value q_i wherein the value of $q_g - q_i$ has the maximum for the given magnetic induction value (Fig. 23). In the event of the possible usage of expression (28) to compute ionized flow conductivity, magnetic induction critical value could be obtained from Eq. (30):

$$B_{\rm cr} = \sqrt{\frac{m_e n_0 k_c \sqrt{q_i k_{\rm dr} W_i}}{k(1-k)e^2 v^2}} \tag{31}$$

It follows from the presented ratio that the critical value of magnetic induction depends on flow parameters, MHD generator and ionizer, and on rate constants of elementary plasma processes. On the other hand, at a fixed value of magnetic induction, it is possible to determine the power density critical value wherein specific ionization costs are equal to the specific power produced by the MHD generator ($q_g = q_i$). From expression (30) for the critical value of specific power, we find [34,35]

$$q_{\rm cr} = \frac{1}{k_{\rm dr} W_i}\left(k(1-k)B^2 v^2 \frac{e^2}{m_e n_0 k_c}\right)^2 \tag{32}$$

In this case, self-sustained mode for MHD generator and ionizer is realized at $q_{\rm cr} > q_i > 0$.

From relation (32) it follows that the existence range of a MPCE self-sustained mode expands with flow velocity increase and gas concentration decrease. Thus, the faster and higher an HFV flies, the more efficient the onboard MHD system's application. Magnetic induction increase also leads to the expansion of the existence range for the self-sustained mode of the MPCE and ionizer.

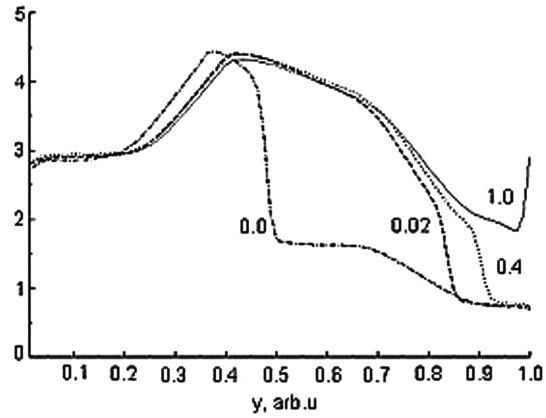

Fig. 24 Density distribution at the channel cross section upstream of a MPCE combustor; $M_\infty = 6$; dynamic pressure equals 3.7×10^4 Pa; values $q_i/q_{\rm cr}$ are indicated adjacent to the curves.

Let us evaluate the value $q_{\rm cr}$, taking advantage of the constant values presented in [25] for elementary processes: $k_{\rm dr} = 1.5 \times 10^{-7}$ cm^3/s, $k_c = 2 \times 10^{-8}$ cm^3/s, and $W_i = 34$ eV for the flow with the following parameters: $v = 2000$ V/s, $T = 300$ K at values $B = 2$ T, and $k = 0.5$. We obtain $q_{\rm cr} = 6.51$ W/cm^3. The value $q_{\rm cr}$ is one of the most important characteristics of MPCE operation conditions.

By way of example, shown in Fig. 24 is the effect of relation $q_i/q_{\rm cr}$ on density distribution at a MHD-controlled inlet in the cross section of the channel upstream of the MPCE combustor. Values $q_i/q_{\rm cr}$ are indicated adjacent to the curves. Flow density increases with a $q_i/q_{\rm cr}$ rise. Under the given conditions for this computation, a significant density increase is achieved even at $q_i/q_{\rm cr} = 0.4$. A further increase of the $q_i/q_{\rm cr}$ relation under these conditions does not result in a significant variation of flow density distribution. Excessive power $q_g - q_i$ left after expenditures for ionizer operation could be realized onboard HFVs for other needs.

Table 3 provides values $q_G^{\max} = q_g - q_i$, which is the maximum power taken off the MHD generator volume unit less the power consumed by the ionizer at different values of temperature, flow velocity, magnetic induction magnitude, and load factor. Working gas pressure is equal to 0.1 atm.

Thus, calculations show that the MHD generator with nonequilibrium conductivity could be realized under conditions typical for HFV flight, with self-sustained mode for the MHD generator and ionizer being subject to excessive power $q_g - q_i$, constituting a considerable part of the MHD generator power.

In closing the section, we shall consider one more important aspect of the MHD generator interaction with other systems onboard HFVs. Because such a generator is a part of MPCE, electric energy production is not the only function it should perform. In line with the Ajax general concept, the MHD generator has to provide for efficient control of MPCE performance. In the succeeding sections, an important MPCE parameter is introduced and substantiated: the

Table 3 Characteristics of the specific excessive power of the MHD generator

T, K	v, m/s	B, T	k	$q_G^{\max}$, MW/m^3
600	2000	1	0.5	4.9
600	2000	2	0.5	77.8
600	3000	1	0.5	24.6
600	3000	2	0.5	394.0
600	2000	1	0.2	2.0
600	2000	2	0.2	31.9
300	2000	1	0.5	1.2
300	3000	2	0.5	98.5

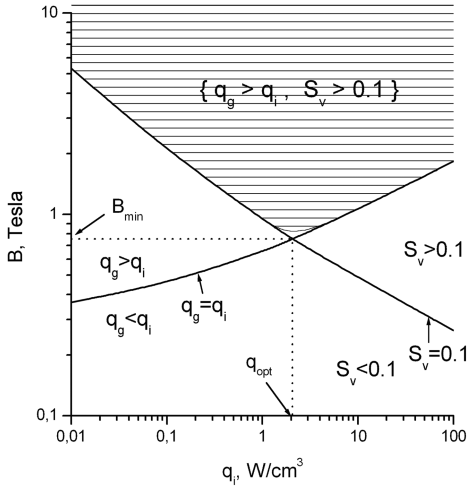

Fig. 25 Region of parameters B and q_i variation wherein self-sustained mode for the MHD generator with nonequilibrium conductivity and the required parameter value of the MHD interaction are simultaneously ensured; the MHD generator is located at section 1 (Fig. 13); $M_\infty = 6$.

so-called parameter of the MHD interaction, $S_v = \sigma B^2 L/\rho v$, where L is the MHD generator length. As will be shown later, to markedly enhance ramjet performance, parameter of the MHD interaction has to meet inequality $S_v > 0.1$. As per this inequality, if we are to decrease the energy supplied to the flow for its ionization, then it is necessary to increase the value of magnetic induction.

Figure 25 depicts the region of parameters B and q_i variation, wherein self-sustained mode for the MHD generator with nonequilibrium conductivity is provided at the same time with the required value of the MHD interaction parameter. The incident curve here corresponds to the permanent value of the MHD interaction parameter $S_v = 0.1$. The rising curve corresponds to critical conditions of the MHD generator for which $q_g = q_i$. Parameters q_i and B corresponding to the points on the plane in the crosshatched region simultaneously meet the self-sustained mode of the MHD generator with nonequilibrium conductivity and the condition of the MHD interaction $S_v > 0.1$. It follows from the presented figure that there exists an optimal value of energy deposition into ionization wherein existence of the required MPCE operating conditions is ensured under the minimum value of magnetic induction.

D. Mathematical Model of General-Type MPCE with Nonequilibrium Flow Ionization System

Here, we examine MPCE with an internal MHD generator and MHD accelerator, wherein the system of nonequilibrium flow ionization is included into the HFV overall energy balance. To mathematically describe the system under consideration, a quasi-one-dimensional approximation is used. In so doing, a quasi-one-dimensional flow model in the MHD generator of the Faraday type is generalized for the case of the Hall generator that would allow a uniform description of ramjet operation with MHD systems of diverse types in a wide range of parameter variation. The flow is assumed to be a stationary one that can be described by the following set of equations [36]:

$$\rho v A = \text{const} \tag{33a}$$

$$\begin{aligned} &\rho v \frac{\mathrm{d}v}{\mathrm{d}x} + \frac{\mathrm{d}p}{\mathrm{d}x} = f_x \equiv [j \times B]_x, \\ &\rho v \frac{\mathrm{d}(h + v^2/2)}{\mathrm{d}x} = j \cdot E, \\ &p = \frac{R_r \rho T}{m_0} \end{aligned} \tag{33b}$$

where ρ is the flow density, v is the flow velocity, p is the static pressure, h is the enthalpy, A is the cross-sectional square of the MHD channel, x is the longitudinal coordinate, B is the magnetic field induction, E is the electric intensity, j is the current density, and f is the volume density of the Lorentz force.

In addition, the variables in question are related to each other through the generalized Ohm law:

$$\mathbf{j} + \mu[\mathbf{j} \times \mathbf{B}] = \sigma(\mathbf{E} + [\mathbf{v} \times \mathbf{B}]) \tag{34}$$

where μ is electron mobility, σ is electric conductivity, and $\mathbf{v}$ is the vector of flow velocity.

The magnetic field configuration is given by the following relation:

$$\mathbf{B} = \{0, B_y, 0\} \tag{35}$$

For the ideal sectionalized MHD generator of the Faraday type, the current field configuration and electric field are given by the relations

$$\mathbf{j} = \{0, 0, j_z\}, \qquad \mathbf{E} = \{0, 0, E_z\} \tag{36}$$

Now let us determine the load factor of the MHD generator through the relation

$$k = -E_z/(v_x \cdot B_y) \tag{37}$$

In the end, we shall obtain the following expressions for the Faraday-type MHD generator:

$$[j \times B]_x = -(1-k)\sigma B^2 v, \qquad (j \cdot E) = -k(1-k)\sigma B^2 v^2 \tag{38}$$

In the case of the Hall generator, the configuration of the current vectors and electric intensity acquires the form of

$$\mathbf{j} = (j_x, 0, j_z), \qquad \mathbf{E} = (E_x, 0, 0), \qquad k = -E_x/(\beta \cdot v_x \cdot B_y) \tag{39}$$

$$\begin{aligned} [j \times B]_x &= -(1-k)B^2\sigma\beta^2 v/(1+\beta^2), \\ (j \cdot E) &= -k(1-k)\sigma B^2 v^2 \beta^2/(1+\beta^2) \end{aligned} \tag{40}$$

where β is the Hall parameter.

In the MHD generator of the Hall type, the Lorentz force has both an x component and a z component. To apply quasi-one-dimensional approximation, it is necessary that their relation would meet inequality:

$$|f_x/f_y| = \beta(1-k)/(1+k\beta^2) \ll 1 \tag{41}$$

In [20,21], analytical solution was obtained for the set of Eqs. (33) in a form suitable for the analysis of complex gasdynamic systems, including MHD systems. It should be particularly emphasized that these solutions may be written in the generalized form suitable for description of both Faraday and Hall MHD generators. Thus, to specify the MHD generator type, it would be sufficient to use only parameter ψ, presented in Table 4.

Taking advantage of the results [20,21], the temperature relation at the outlet and intake of the MHD generator is given by the general type of expression:

$$T_2/T_1 = 1 + (1+\xi)\omega\eta\psi \tag{42}$$

where η is the enthalpy extraction ratio, ξ is the factor specifying the flow regime, and magnitude ω has the following form:

$$\omega = M_1^2(\gamma - 1)/2 + 1 \tag{43}$$

Table 4 Parameter ψ values for Faraday and Hall generators

Generator type	Parameter Ψ
Faraday	$\frac{1}{k} - 1$
Hall	$(1 + \beta^2 k^2)/\beta^2 k(1-k)$

Table 5 Parameter ξ values for some flow conditions in the channel of the MHD general type of generator

Flow conditions	MHD generator type	
	Faraday	Hall
$\rho = \text{const}$	$\gamma - 1$	$\gamma - 1$
$P = \text{const}$	0	0
$T = \text{const}$	-1	-1
$M = \text{const}$	$-1 - k/(\omega(1-k))$	$-1 - \beta^2 k(1-k)/(\omega(1+\beta^2 k^2))$
$v = \text{const}$	$-1/(1-k)$	$-(1+\beta^2 k)/(1+\beta^2 k^2)$

where M_1 is the Mach number at the MHD generator entrance, and γ is the ratio of gas specific heat at constant pressure to specific heat at constant volume. Parameter ξ values for some specific flow conditions are given in Table 5, in which an ξ value of 0 corresponds to constant static pressure along the channel, and the case $\xi > 0$ conforms to a pressure increase lengthwise of the channel.

Condition $\rho v A = \text{const}$ sets the cross-sectional area of the MHD channel as a function of the x coordinate at the given ξ value. In this case, $A = \text{const}$ is well described if $\xi = \xi(\psi)$, where

$$\xi(\psi) = \gamma - 1 + (\gamma + 1/\psi)/(M_1^2 - 1)$$

To further investigate the existence limits of self-sustained mode for the MHD generator with nonequilibrium conductivity, we introduce the following variables: Q_i is the power supplied to the MHD generator channel for flow ionization purposes, and Q_g is the power produced by the MHD generator.

We also enter a designation for these two magnitude's ratio:

$$r = Q_i/Q_g \tag{44}$$

It is evident that the self-sustained regime is realized at $r < 1$.

The energy produced by the MHD generator may be written in terms of the variables introduced earlier, in the form:

$$Q_g = -\int_0^L (j \cdot E) A(x)\, \mathrm{d}x \tag{45}$$

Previously introduced was parameter q_i, specifying the power spent for ionization of the flow volume unit. If this parameter is constant across the whole volume of the MHD generator channel, we have for Q_i

$$Q_i = q_i V \tag{46}$$

where V is the volume of the MHD generator channel.

To find the dependence of the enthalpy extraction ratio on the MHD generator length at the given parameter ξ value, it is necessary to specify the ionizer type along with the developed model of nonequilibrium conductivity. Well known are diverse techniques for nonequilibrium conductivity production (e.g., use of various gas discharges, microwave radiation, and high-energy charged particle beams).

Taking advantage of Eq. (29) for volume specific power produced by the MHD generator, as per [20,23], we have

$$r(\eta) = \sqrt{\frac{q_i}{q_{\mathrm{cr}}}} \cdot \frac{1}{\eta} \int_0^\eta \frac{G(\psi,\xi,M_1,\eta')^D}{Z(k,\psi,M_1,\eta')}\, \mathrm{d}\eta'$$

$$G(\psi,\xi,M,\eta) = 1 + \psi(1+\xi)\left(1 + \frac{\gamma-1}{2}M^2\right)\eta$$

$$Z(\psi,\xi,M,\eta) = 1 - (1+\psi(1+\xi))\frac{2+(\gamma-1)M^2}{(\gamma-)M^2}\eta \tag{47}$$

$$D = \frac{\gamma}{\gamma-1}\frac{\xi}{\xi+1} - 1 \qquad q_{\mathrm{cr}} = \frac{1}{w_i k_{\mathrm{dr}}}(k(1-k)\chi\mu e B^2 v_1^2)^2$$

$$\chi = \begin{cases} 1, & \text{Faraday case} \\ \beta^2/(1-\beta^2), & \text{Hall case} \end{cases}$$

In the event of c_p constant value, parameters η and q_g are connected by the relation

$$q_g = \varphi c_p T_1 \left(1 + \frac{\gamma-1}{2}M_1^2\right)\eta \tag{48}$$

where ϕ is the mass flow rate, and T_1 is the temperature at the MHD generator input.

In the limit $\eta \to 0$, parameter $r \to (q_i/q_{\mathrm{cr}})^{1/2}$, which coincides with the result obtained in local approximation in [22]. Equations (47) describe requirements to the ionizer and MHD generator in terms of self-sustained operational mode maintenance.

The coefficient of flow energy conversion into electric energy is but one of the parameters that characterize a degree of the MHD system's interaction with ionized flow. One more feature of importance is the transformation degree of free flow impulse by the MHD system. This magnitude, called the *MHD interaction parameter*, is determined by the relation

$$S_v = \frac{\sigma B^2 L}{\rho v} \tag{49a}$$

where L is the MHD channel length.

MHD interaction parameter S_v and enthalpy extraction ratio η are connected by the relation [20]

$$S_v = \frac{1 + [(\gamma-1)/2]M_1^2}{k(1-k)(\gamma-1)\chi M_1^2} \int_0^\eta \frac{G(k,\xi,M_1,\eta')^{2A}}{\sqrt{Z(k,\xi,M_1,\eta')}}\, \mathrm{d}\eta' \tag{49b}$$

where variables S_v, σ_1, ρ_1, and v_1 correspond to MHD generator input.

In Figs. 26 and 27, a type of function $r(\eta)$ for Faraday and Hall generators at various values of M_1 and load factor k is shown. For all MHD cases, the flow is characterized by the value $\xi = \xi(\psi)$. It can be seen that function $r(\eta)$ is monotonically rising. Value $\eta = \eta^*$, specified by relation $r(\eta^*) = 1$, gives the upper limit for the enthalpy extraction ratio wherein the self-sustained operational mode of the MHD generator and ionizer exist.

It can be seen that the η^* value for the Faraday generator exceeds the value for the Hall generator at the same conditions. From the presented dependences, it follows that the region of self-sustained mode existence expands for both generator types with a Mach number increase. Simultaneously, the load-factor increase narrows the region of self-sustained operational mode existence for the Faraday generator and expands it for the Hall generator.

The development of the MPCE mathematical model made possible a uniform description of scramjet operation equipped with various MHD systems in a wide range of MPCE parameter variation and determination of their basic values and dependencies for

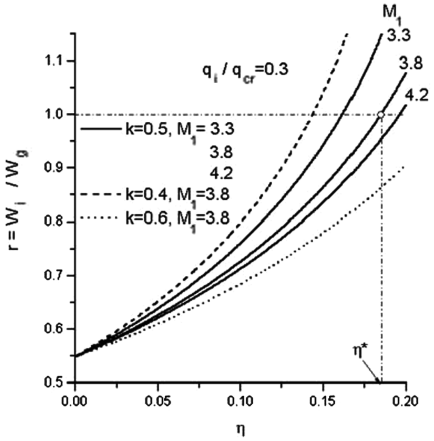

Fig. 26 Relative power spent for flow ionization in the channel of the MHD generator as a function of the enthalpy extraction ratio for various Mach number and load-factor values: Faraday MHD generator.

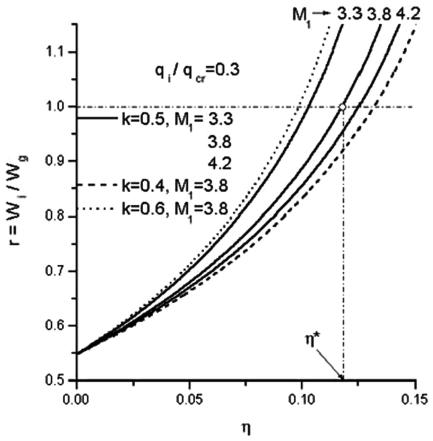

Fig. 27 Relative power spent for flow ionization in the channel of the MHD generator as a function of the enthalpy extraction ratio for various Mach number and load-factor values: Hall MHD generator.

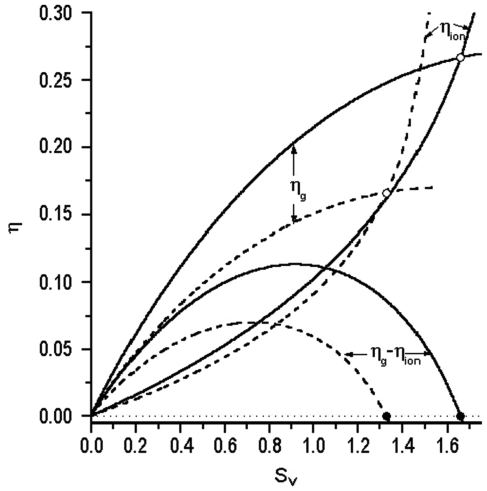

Fig. 28 Dependence of η on S_v for $\beta = 2$, $M_0 = 6$, $M_d = 10$, $\theta_N = 15\,\text{deg}$, $F_{\text{th}} = 0.12$, $q_i/q_{\text{cr}} = 0,05$, $\xi_1 = 0.5$, $k_1 = 0.5$, and $k_3 = 1.2$.

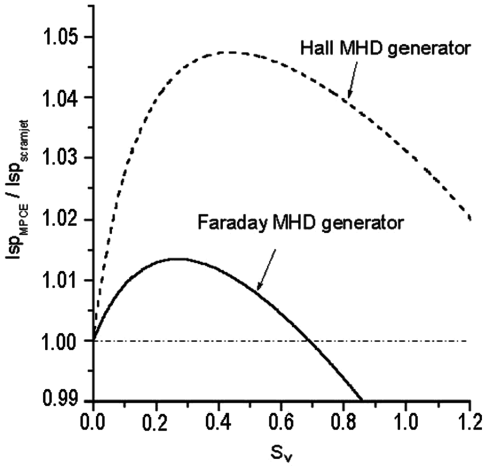

Fig. 29 Dependence of relative specific MPCE impulse on the MHD interaction parameter for Hall-type and Faraday-type generators at $\beta = 2$. $M_0 = 6$, $M_d = 10$, $\theta_N = 15\,\text{deg}$, $F_{\text{th}} = 0.12$, $q_i/q_{\text{cr}} = 0.05$, $\xi_1 = 0.5, k_1 = 0.5$, and $k_3 = 1.2$.

different operational regimes, serving as a solid base for propulsion designs.

Thus, physical restrictions to the realization of principles of the MHD control over scramjet performance are associated, first of all, with the problem of ensuring self-sustained operational mode for the MHD generator with nonequilibrium conductivity. Their identification allowed the formulation of basic requirements to the parameters of the MHD system and ionizer. Inequality $q_g > q_{0\text{cr}}$ sets the lower limit to the MHD generator specific power, and inequality $r(\eta^*) < 1$ sets the upper limit to the enthalpy extraction ratio.

E. Investigation of Physical Restrictions on Scramjet MHD Control

Now we come to the consideration of conditions for the realization of principles for scramjet MHD control wherein enhancement of MPCE performance occurs. Along with ensuring self-sustained operational mode, MHD interaction has to be powerful enough to provide for a significant increase of the scramjet specific impulse. Let us consider the MPCE subsystem consisting of an air inlet, MHD generator, and MHD accelerator [37–39]. The geometry of the inlet under investigation and its parametrization correspond to Fig. 13. When computing, the inlet throat F_{th} parameter varied in the range os 0.08–0.17 at Mach number $M_0 < M_d$. The degree of the MHD system's effect on the flow could be characterized by the two dimensionless quantities: the MHD interaction parameter, previously spoken of, and the coefficient of flow energy conversion into electric power for the MHD generator. To describe the energy characteristics, we enter the parameters

$$\eta_g = Q_g/Q_0, \qquad \eta_i = Q_i/Q_0 \tag{50a}$$

where

$$Q_0 = \varphi c_p T_0[1 + M_0^2(\gamma - 1)/2] \tag{50b}$$

is the flow enthalpy, Q_g is the power produced by the MHD generator, and Q_i is the power spent for flow ionization.

To describe the power characteristics, the relation of specific MPCE impulse to specific scramjet impulse has been used, which corresponds to the MPCE with a zero value of magnetic induction:

$$I^*_{\text{sp}} = I^{\text{MPCE}}_{\text{sp}}/I^{\text{scramjet}}_{\text{sp}} \tag{51}$$

Parameter S_v of the MHD interaction has been considered as an independent variable. The results of numerical computation of the characteristics at hand are presented in Figs. 28–33.

In Fig. 29, dependencies of η parameters on the MHD interaction parameter for Faraday and Hall generators with nonequilibrium conductivity are provided. The point of intersection for the curves η_g and η_i corresponds to the maximum (at preset conditions) value of the MHD interaction parameter wherein MPCE self-sustained operational mode might be realized. Solid lines correspond to the Faraday-type generator and dotted lines correspond to the Hall-type generator version. In this case, power excess $Q_{\text{ex}} = (\eta_g - \eta_i)Q_0$ may be formed in the system that could be used for onboard systems' supply. From the presented dependencies, it follows that from the energy standpoint, the Faraday-type generator is preferable to Hall-type generator.

Figure 28 illustrates the investigation results regarding the specific-impulse properties of a MPCE with Faraday- and Hall-type MHD generators. The solid line corresponds to the Hall-type generator and the dotted line corresponds to the Faraday-type generator. As the computational results show, under the same conditions, the Hall MHD generator provides for a larger specific impulse than with the Faraday MHD generator. In all cases under consideration, flow conditions are specified by the function $\xi = \xi(\psi)$.

The dependence of specific impulse and relative excess power on Hall parameter β for MPCE with the Hall generator is shown in Figs. 30 and 31. The dotted curve corresponds to the Faraday generator. From the presented dependencies, it follows that with parameter β, enhancement characteristics of a MPCE with the Hall MHD generator approach characteristics of a MPCE with the Faraday MHD generator.

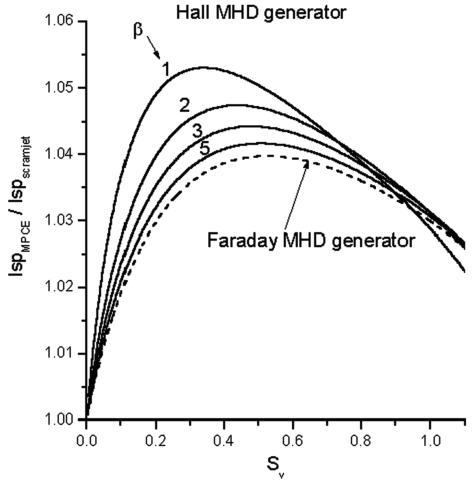

Fig. 30 Dependence of relative specific impulse for MPCE with Hall-type generator on Hall parameter β at $M_0 = 6$, $M_d = 10$, $\theta_N = 15\,\text{deg}$, $F_{\text{th}} = 0.12$, $q_i/q_{\text{cr}} = 0.05$, $\xi_1 = \xi(\psi)$, $k_1 = 0.5$, and $k_3 = 1.2$.

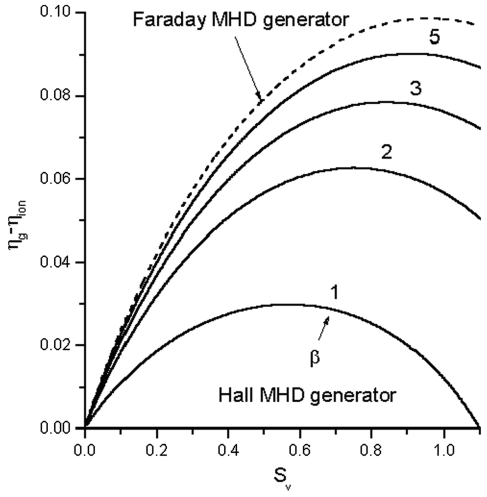

Fig. 31 Dependence of relative power excess on the MHD interaction parameter of a MPCE with Hall-type generator for various values of the Hall parameter β at $M_0 = 6$, $M_d = 10$, $\theta_N = 15\,\text{deg}$, $F_{\text{th}} = 0.12$, $q_i/q_{\text{cr}} = 0.05$, $\xi_1 = \xi(\psi)$, $k_1 = 0.5$, and $k_3 = 1.2$.

Figures 32a and 32b illustrate the dependence of a MPCE specific impulse on the MHD interaction parameter and load factor. Values of factor k_1 are presented alongside the appropriate curves. As the presented results show, in the case of the Faraday MHD generator, the specific impulse increases with the decrease of load factor at small values of the MHD interaction parameter S_v. In the case of the Hall MHD generator, on the contrary, the specific impulse increases with load-factor increase. With the MHD interaction parameter increase, dependence of the specific impulse on the load factor becomes nonmonotonic for generators of both types.

The dependence of relative power excess on the MHD interaction parameter at various load-factor values for the MHD generator has also been investigated. Appropriate curves are presented in Fig. 33 for MPCE with the MHD generator of the Faraday and Hall types. As the presented results indicate, both families of curves for Faraday and Hall cases are close to each other. Our attention have been engaged by the fact that the Faraday curve characterized by load factor $k_1 = k_1^F$ is close to the Hall curve with a load factor of the type $k_1^H = 1 - k_1^F$.

The same characteristics for MPCE with MHD generators of different types are correlated in Figs. 34 and 35. From Fig. 34 it follows that at the given conditions, the specific impulse of a MPCE with the MHD Hall generator exceeds that of a MPCE with the Faraday generator. The curves are very close to each other only for

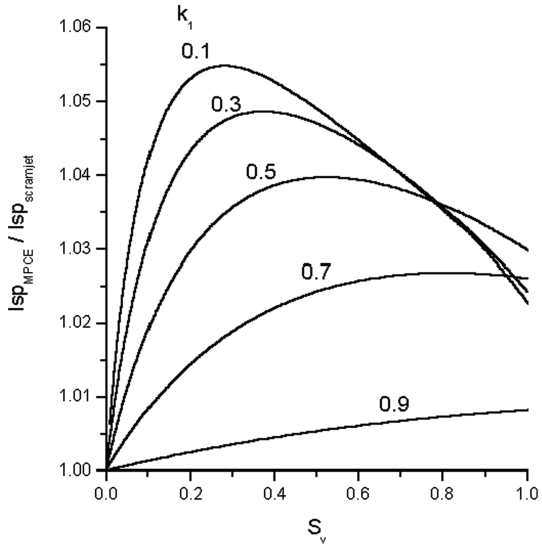

a)

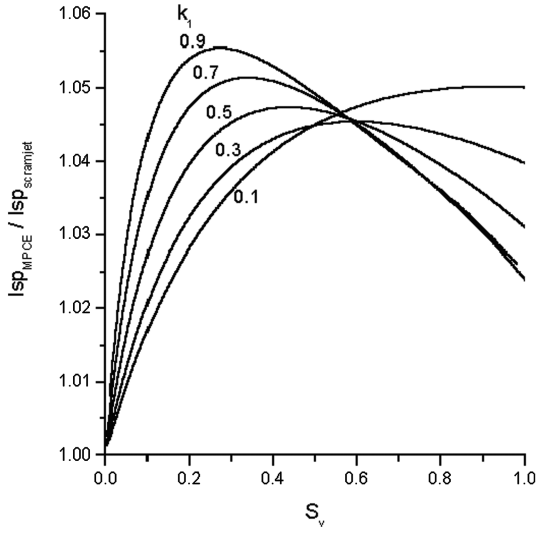

b)

Fig. 32 Dependence of a MPCE specific impulse on the MHD interaction parameter at various values of load factor k_1 for a) Faraday and b) Hall MHD generators; $M_0 = 6$, $M_d = 10$, $\theta_N = 15\,\text{deg}$, $F_{\text{th}} = 0.12$, $q_i/q_{\text{cr}} = 0.05$, $\xi_1 = \xi(\psi)$, and $k_3 = 1.2$; for the Hall generator, parameter $\beta = 2$.

load factors of the types $k_1^H = 0.9$ and $k_1^F = 0.1$. At the same time, as it follows from Fig. 35, MPCE with the Faraday generator produces more electric energy than is the case with the Hall-type generator throughout the range of the MHD interaction parameter variation.

The results of investigation on the dependence of a MPCE specific impulse on the MHD interaction parameter at various parameters of inlet throat F_{th} are shown in Fig. 36. Analogical dependencies on the enthalpy extraction ratio are presented in Fig. 37. It is obvious that the larger quantity F_{th}, the stronger positive effect of the MHD interaction parameter upon the propulsion specific impulse. It can be explained by the fact that the flow experiences supplementary MHD compression because parameter $\xi > 0$. At small values of the MHD interaction parameter, the Hall MHD generator offers a more significant increase of the propulsion specific impulse in comparison with the Faraday MHD generator. True, at $S_v > 0.7$, the Faraday MHD generator provides a larger increment in the propulsion specific impulse than does the Hall MHD generator. From Fig. 36 it follows that the larger the F_{th} quantity, the higher the value of enthalpy extraction ratio η_g. But in all cases, the Faraday generator is more powerful than the Hall generator.

Figures 38 and 39 present the results of an investigation into the dependence of the relative specific impulse and relative power excess

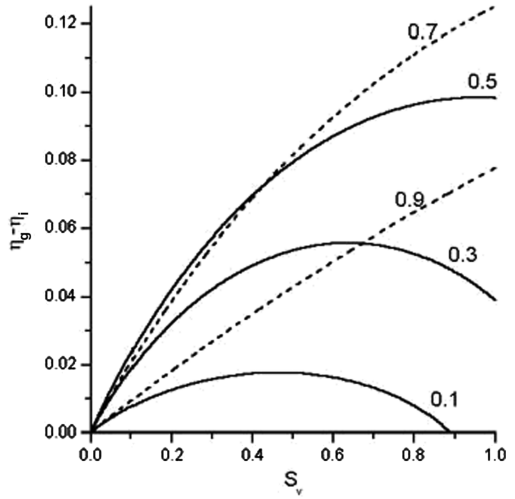

a)

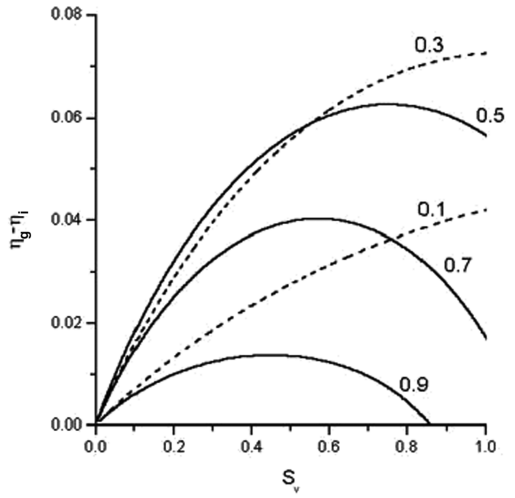

b)

Fig. 33 Dependence of relative energy excess on the MHD interaction parameter at various values of load factor k_1 for a) Faraday and b) Hall generators; $M_0 = 6$, $M_d = 10$, $\theta_N = 15\,\text{deg}$, $F_{\text{th}} = 0.12$, $q_i/q_{\text{cr}} = 0.05$, $\xi_1 = \xi(\psi)$, and $k_3 = 1.2$; for the Hall generator, parameter $\beta = 2$.

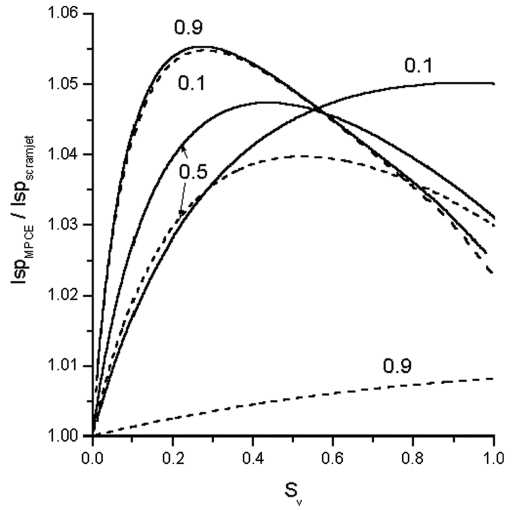

Fig. 34 Dependence of a MPCE specific impulse on the MHD interaction parameter for different MHD generator types at various values of load factor k_1 at $M_0 = 6$, $M_d = 10$, $\theta_N = 15\,\text{deg}$, $F_{\text{th}} = 0.12$, $q_i/q_{\text{cr}} = 0.05$, $\xi_1 = \xi(\psi)$, and $k_3 = 1.2$; load-factor values are indicated adjacent to the curves; the solid curve is the Hall-type generator ($\beta = 2$) and the dotted curve is the Faraday-type generator.

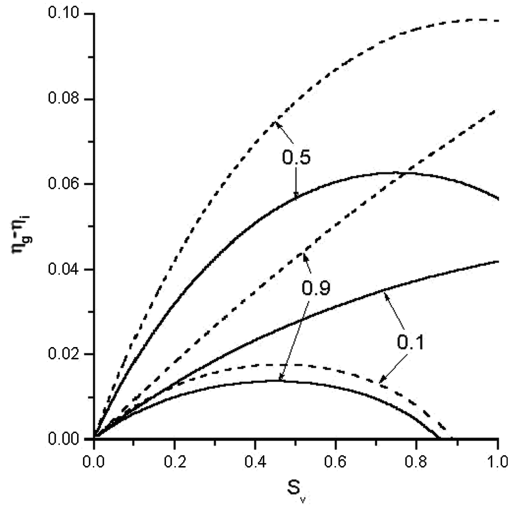

Fig. 35 Dependence of MPCE power excess on the MHD interaction parameter for different generator types at various load-factor values k_1 at $M_0 = 6$, $M_d = 10$, $\theta_N = 15\,\text{deg}$, $F_{\text{th}} = 0.12$, $q_i/q_{\text{cr}} = 0.05$, $\xi_1 = \xi(\psi)$, and $k_3 = 1.2$; load-factor values are indicated adjacent to the curves; the solid curve is the Hall-type generator ($\beta = 2$) and the dotted curve is the Faraday-type generator.

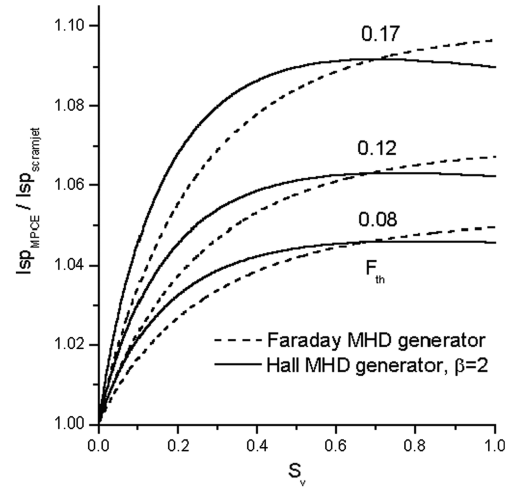

Fig. 36 Dependence of a MPCE relative specific impulse on the MHD interaction parameter at various values of inlet throat F_{th} at $M_0 = 6$, $M_d = 10$, $\theta_N = 15\,\text{deg}$, $q_i/q_{\text{cr}} = 0$, $\xi_1 = \xi(\psi)$, $k_1 = 0.5$, and $k_3 = 1.2$.

on the MHD interaction parameter at various values of relation q_i/q_{cr}. The solid lines correspond to the Hall generator and the dotted lines correspond to the Faraday generator. In line with theoretical results, quantity q_{cr} is proportional to β^4 and, consequently, a magnetic induction increase leads to the prompt decrease of relation q_i/q_{cr} and therefore to an increase of the MPCE specific impulse and relative power excess value $\eta_g - \eta_{\text{cr}}$.

Analysis of the presented dependencies of a number of MPCE characteristics on the MHD interaction parameter S_v (Figs. 38–42) shows that to noticeably improve ramjet performance it is necessary to ensure value $S_v \geq 0, 1$. It can be concluded by results presented in this section that the MHD interaction leads to improvement of MPCE performance only in the event that the MHD subsystems would comply with the following inequalities:

$$\begin{aligned} &\xi_1 > \frac{T_1}{\Delta T}\cdot\left[1+\frac{1}{\psi}\left(1-\frac{1}{k_3}\left(1-\sqrt{\frac{q_{\text{ion}}}{q_{\text{cr}}}}\right)\right)\right], \\ &\gamma - 1 + \frac{\gamma + 1/\psi}{M_1^2 - 1} > \frac{T_1}{\Delta T}\cdot\left[1+\frac{1}{\psi}\left(1-\frac{1}{k_3}\left(1-\sqrt{\frac{q_{\text{ion}}}{q_{\text{cr}}}}\right)\right)\right] \end{aligned} \tag{52}$$

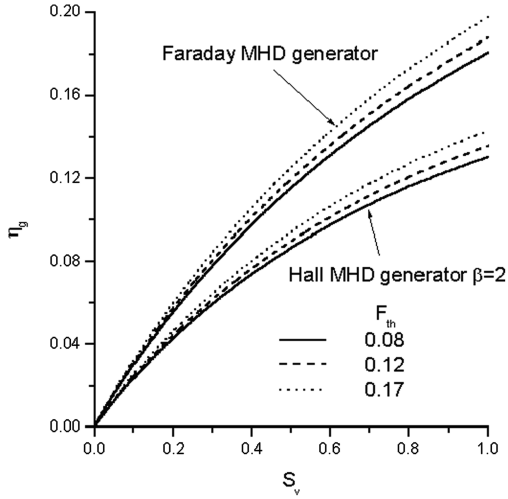

Fig. 37 Enthalpy extraction ratio as a function of the MHD interaction parameter for various inlet throat parameter values F_{th} and MHD generator different types at $M_0 = 6$, $M_d = 10$, $\theta_N = 15\,\text{deg}$, $q_i/q_{\text{cr}} = 0$, $\xi_1 = \xi(\psi)$, $k_1 = 0.5$, and $k_3 = 1.2$.

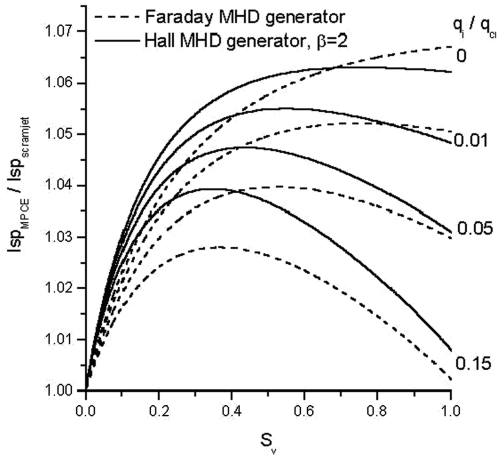

Fig. 38 Dependence of a MPCE relative specific impulse on the MHD interaction parameter for various values q_i/q_{cr} at $M_0 = 6$, $M_d = 10$, $\theta_N = 15\,\text{deg}$, $F_{\text{th}} = 0.12$, $\xi_1 = \xi(\psi)$, $k_1 = 0.5$, and $k_3 = 1.2$.

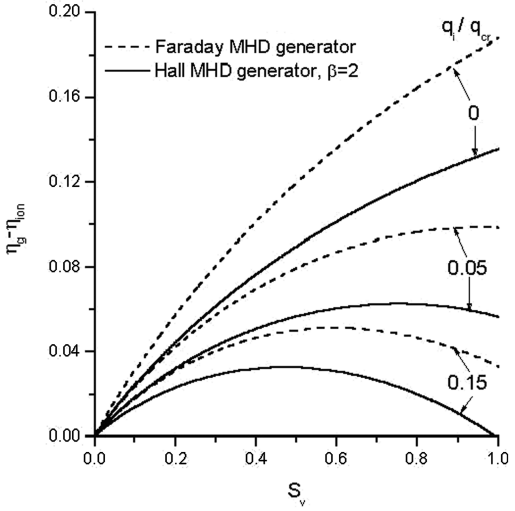

Fig. 39 Dependence of MPCE relative power excess on the MHD interaction parameter for various values q_i/q_{cr} at $M_0 = 6$, $M_d = 10$, $\theta_N = 15\,\text{deg}$, $F_{\text{th}} = 0.12$, $\xi_1 = \xi(\psi)$, $k_1 = 0.5$, and $k_3 = 1.2$.

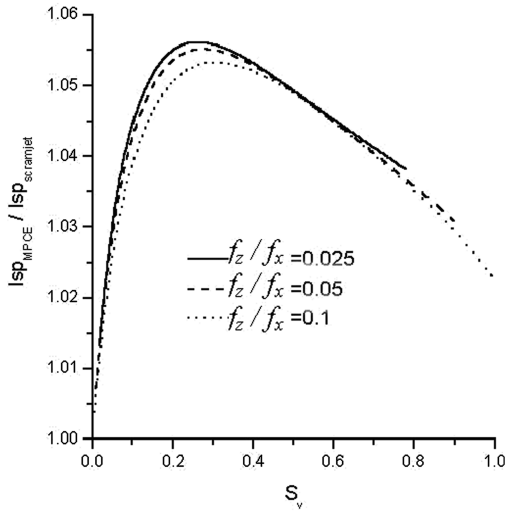

Fig. 40 Dependence of relative specific impulse for MPCE with the Hall generator on the MHD interaction parameter for various component relations fz/fx at $M_0 = 6$, $M_d = 10$, $\theta_N = 15\,\text{deg}$, $F_{\text{th}} = 0.12$, $q_i/q_{\text{cr}} = 0.05$, $\xi_1 = \xi(\psi)$, $k_1 = 0.5$, $k_3 = 1.2$, and $\beta = 2$.

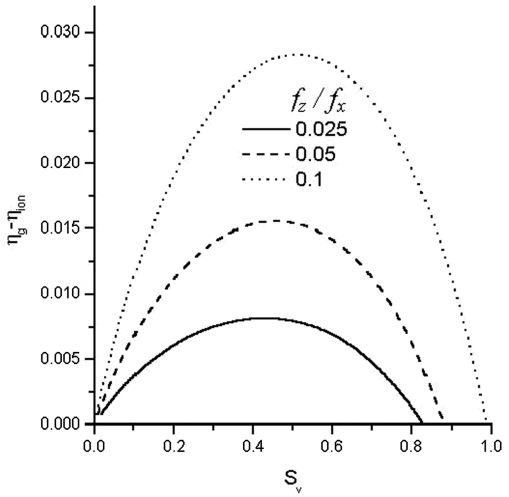

Fig. 41 Dependence of relative power excess for MPCE with the Hall generator on the MHD interaction parameter for various component relations fz/fx at $M_0 = 6$, $M_d = 10$, $\theta_N = 15\,\text{deg}$, $F_{\text{th}} = 0.12$, $q_i/q_{\text{cr}} = 0.05$, $\xi_1 = \xi(\psi)$, $k_1 = 0.5$, $k_3 = 1.2$, and $\beta = 2$.

The dependence of ramjet performance on the MHD system's effect is specified to a considerable degree by such parameters as the MHD generator type, air inlet characteristics, load factors, Hall parameter, ionizer, and flow parameters. These are precisely the parameters that govern the conditions wherein the MHD system's application could result in a substantial improvement of ramjet performance.

Growth of the propulsion specific impulse is achieved bya relation q_i/q_{cr} decrease: either by q_i decrease or by q_{cr} increase. At q_i decrease, flow conductivity drops; therefore, to ensure significant MHD effect, it is necessary to increase the length of the MHD generator channel. On the other hand, to increase critical power q_{cr}, it is necessary to increase magnetic induction that, in principle, could prove unfeasible from a technical point of view.

The existence condition for self-sustainable mode $0 < r = Q_i/Q_g < 1$ imposes limitations on the MHD interaction parameter that it has to exceed some limiting value S^*. Condition $r(S^*) = 1$ gives the limiting value $q_i = U(S^*, k_1, M_1, \xi_1)q_{\text{cr}}$ and limiting value for magnetic induction above which self-sustained mode ($B > B_{\text{lim}}$) sets in:

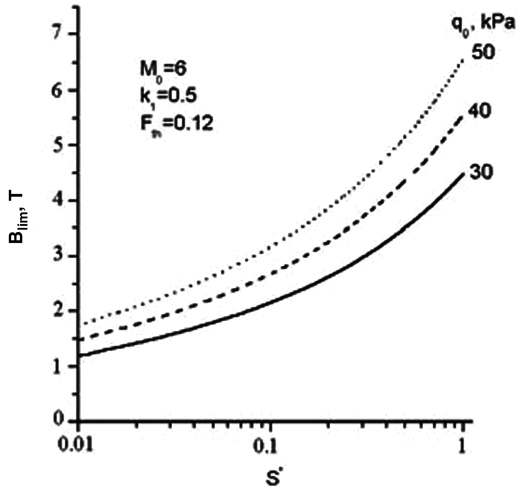

a)

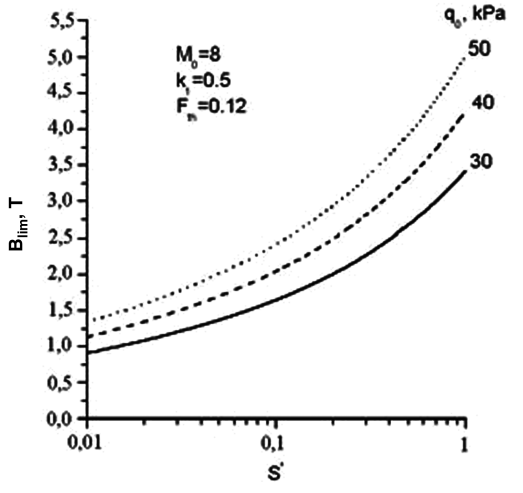

b)

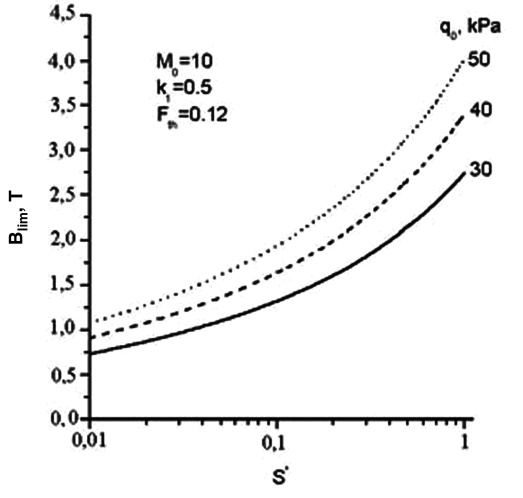

c)

Fig. 42 Limiting value of magnetic induction as a function of the MHD interaction parameter.

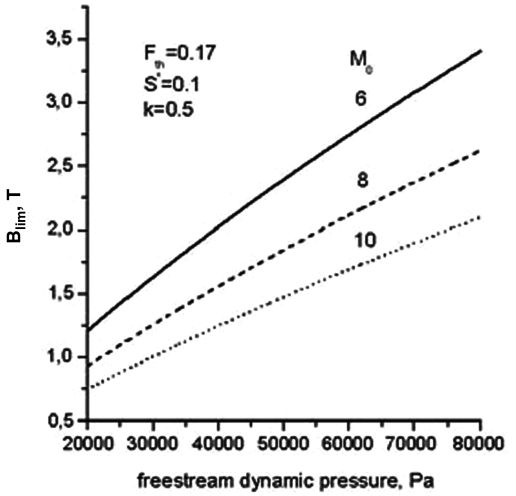

a)

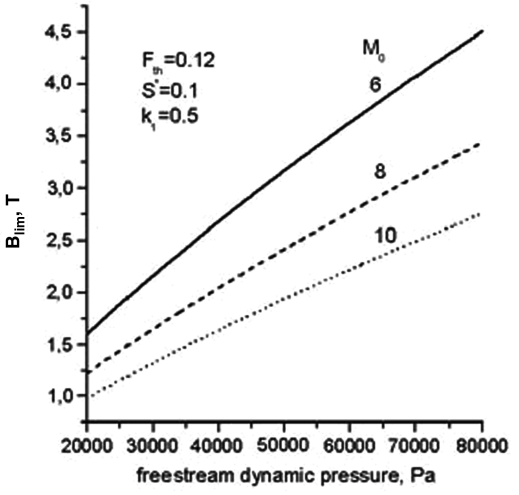

b)

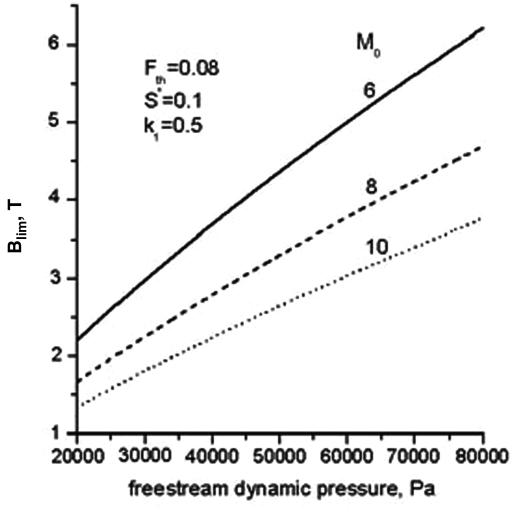

c)

Fig. 43 Limiting value of magnetic induction as a function of freestream dynamic pressure.

$$B_{\lim} = [(S^* \rho_1^3 / L v_1 k_1 (1 - k_1)) \times ((m_e/m_0)^2 W_i k_c^2 k_{\mathrm{dr}})/(e^4 U(S^*, k_1, M_1, \xi_1)^{1/2})]^{1/4}$$

where m_0 is the gas molecular mass. Value $B_{\lim}$ decreases with parameters S^*, ρ_1 decreases, and parameters L and v_1 increase.

Figures 42 and 43 provide calculated dependencies of the limiting value for magnetic induction on the MHD interaction parameter and freestream dynamic pressure, with the air inlet geometry defined by the parameters $M_d = 10$, $\theta_N = 15$ deg, and $F_{\mathrm{th}} = 0.1$.

The calculated values of limiting magnetic induction for the internal MHD generator with some inlet configurations, various

Mach numbers, and freestream dynamic pressure are indicative of the physical feasibility of HFV self-sustained flight conditions. The higher and faster the hypersonic flight, the easier it is to realize MHD control over a ramjet with nonequilibrium conductivity.

IV. Conclusions

The performed investigation on the substantiation of the possible usage of MHD systems in a scramjet channel and their application with hypersonic technologies for control over HFV aerodynamic performance proved their feasibility following the development of a MPCE and some technical solutions, such as those listed next: 1) a concept of the MHD generator application for airflow deceleration and scramjet efficiency enhancement, 2) a concept of the MHD generator application for control over mass airflow rate and the flow structure in the scramjet inlet, and 3) a concept and mathematical model of the MHD generator on cold airflow with nonequilibrium conductivity.

The MHD system's application for deceleration and compression of the airflow and scramjet efficiency enhancement has been carried out on the basis of analysis of the MPCE system, consisting of the inlet, internal Faraday MHD generator, combustion chamber, MHD accelerator, and nozzle. General expressions for the specific impulse as a function of many MPCE parameters have been obtained. The region of their variation wherein the MHD system allows an increase of propulsion specific impulse has been studied. Its dependence on the MHD generator load factor is maximum, corresponding to the inlet with the minimum value of the flow turning angle. It is shown that a MPCE impulse increase is subject to a pressure increase lengthwise of the MHD generator channel.

When developing the conception of the MHD generator application for control over mass flow rate and flow structure in the inlet, conditions have been studied that differed considerably from the design conditions. Analysis of flowfields in the MPCE controllable inlet carried out in two-dimensional Euler approximation has shown that the MHD effect on the flow results in their considerable modification. Such an effect allows a significant increase of mass flow rate (up to 37%) and thrust (up to 50%). Maximal specific-impulse increase in the considered case reached 12%. It is shown that the MHD effect on the flow makes it possible to manufacture a controllable inlet, thus ensuring the creation of a scramjet capable of efficient operation in a wide range of hypersonic velocities. At the same time, there is no longer need any to use difficult techniques of mechanical control over propulsion geometrical parameters. The farther flight conditions are from the design conditions, the more significant the positive MHD effect.

When developing the conception and structure of the MHD generator on cold airflow with nonequilibrium ionization, a notion of self-sustained operational mode for onboard MHD generator has been introduced, because the mode wherein power produced by the generator exceeded the energy spent by the ionizer for ensuring the required flow conductivity. It is shown that the MPCE self-sustained operational mode is provided for if some critical values of the power density and magnetic field of the MHD generator are in excess. It is illustrated that a magnetic induction increase leads to a significant enhancement of power produced by the MHD generator and range expansion for self-sustained operational mode of a MPCE with nonequilibrium conductivity. For various values of temperature, flow velocity, magnetic induction, and load factor of the MHD generator, computations of maximum power from its volume unit less the power consumed by the ionizer have been performed. It is shown that the MHD generator with nonequilibrium conductivity could be realized under conditions typical for HFV atmospheric flight.

A mathematical model of a MPCE was made wherein the supporting system for the flow nonequilibrium ionization was included in the HFV general energy balance. Realization of such a model in the form of a quasi-one-dimensional model of the flow with nonequilibrium conductivity in the MHD generator, applicable both to Faraday and Hall generators, allowed a uniform description of scramjet operation with various MHD systems in a wide range of MPCE parameter variations. With the selection of an electron beam as the ionizer, flow conductivity dependence on the power deposited into a volume unit has been obtained. The dependence of the enthalpy extraction ratio on the MHD generator length has been analyzed and the variation region for ionization system parameters has been found wherein MPCE self-sustained operational mode is realized. As a result, the parameter of the MHD interaction degree has been defined and its association with enthalpy extraction ratio has been revealed. For Hall and Faraday MHD generators, the boundaries of the enthalpy extraction ratio were found above which self-sustained operational mode of the MHD generator comes into existence. It is shown that in the case of the Faraday MHD generator, this mode existence boundary is higher than with the Hall generator case under the same conditions. With a Mach number increase, the region of self-sustained mode is expanded for both generator types. An increase in the load factor results in the region narrowing for the Faraday MHD generator and expanding for the Hall generator type.

Physical limits to the realization of the MHD control over the scramjet have been investigated, and basic requirements to the parameters of the MHD systems and ionizer wherein enhancement of MPCE performance occurs have been formulated. In terms of energy, the Faraday generator is preferred to the Hall generator, though the latter ensures a higher specific impulse. With the Hall parameter increase, the difference between the two generator performance decreases. Growth of the propulsion specific impulse is achieved through an ionization cost decrease or by the MHD generator critical-power increase. In the first case, flow conductivity drops; therefore, to ensure a significant MHD effect, it is necessary to increase the MHD generator channel length. In the second case, it is necessary to increase magnetic induction, and that might prove technically infeasible. The condition of self-sustained mode existence imposes limits to the MHD interaction parameter. The dependence of the limiting value for magnetic induction on the limiting MHD interaction parameter, MHD channel length, density, and velocity of the flow in the inlet throat has been identified. Values of this quantity calculated for some inlet configurations with various Mach numbers and freestream dynamic pressure testify to the physical feasibility of a hypersonic vehicle flight under self-sustained conditions. It was established that the higher and faster the HFV flight, the easier it is to realize MHD control over a ramjet with nonequilibrium conductivity.

References

[1] Gurijnov, E. P., and Harsha, P. T., "Ajax: New Direction in Hypersonic Technology," AIAA Paper 96-4609, 1996.

[2] Turchak, A. A., Fraishtadt, V. L., and Kuranov, A. L., "New Hypersonic Technologies Under the 'Ajax' Concept," *Poliot*, No. 9, 1999, pp. 3–7.

[3] Kuranov, A. L., Korabelnikov, A. V., Kuchinsky, V. V., and Sheikin, E. G., "Fundamental Techniques of the 'Ajax' Concept: Modern State of Research," AIAA Paper 2001-1915, 2001.

[4] Korabelnikov, A. V., and Kuranov, A. L., "Thermochemical Conversion of Hydrocarbon Fuel Under the 'Ajax' concept," AIAA Paper 99-4921, 1999.

[5] Korabelnikov, A. V., and Kuranov, A. L., "Thermal Protection of Hypersonic Flight Vehicle Using Chemical Heat Regeneration," AIAA Paper 2002-0913, 2002.

[6] Lander, H., and Nixon, A. S., "Endothermic Fuels for Hypersonic Vehicles," AIAA Paper 68-997, 1968.

[7] Siebenhaar, A., Chek, F. F., Karpuk, M., and Edwards, T., "Engineering Scale Titanium Endothermic Fuel Reactor Demonstration for Hypersonic Scramjet Engine," AIAA Paper 99-4909, 1999.

[8] Kurganov, V. A., Zeigarnik, Yu. A., Korabelnikov, A. V., and Maslakova, T. V., "Thermochemical Principle of Cooling Based on Steam Reforming of Methane," *Thermal Engineering (Translation of Teploenergetika (Moscow))*, Vol. 43, No. 3, 1996, pp. 15–19.

[9] Shljahtenko, S. M. (ed.), *The Theory and Calculation of Propulsion Jet Engines*, Moscow, 1987.

[10] Andrews, E. H., Trexler, C. A., and Emami, S., "Tests of Fixed-Geometry Inlet-Combustor Configuration for Hydrocarbon-Fueled Dual-Mode Scramjet," AIAA Paper 94-2817, 1994.

[11] Fraishtadt, V. L., Kuranov, A. L., and Sheikin, Y. G., "Application of the MHD Systems on the Hypersonic Flight Vehicles," *Journal of*

Technical Physics, Vol. 68, No. 11, 1998, pp. 43–47.

[12] Shneider, M. N., Macheret, S. O., and Miles, R. B., "Analysis of Magnetohydrodynamic Control of Scramjet Inlets," *AIAA Journal*, Vol. 42, No. 11, 2004, pp. 2303–2310. doi:10.2514/1.3998

[13] Shneider, M. N., and Macheret, S. O., "Modeling of Plasma Virtual Shape Control of Ram/Scramjet Inlet and Isolator," *Journal of Propulsion and Power*, Vol. 22, No. 2, Mar–Apr. 2006, pp. 447–454. doi:10.2514/1.16959

[14] Kopchenov, V., Vatazhin, A., and Gouskov, O., "Estimation of Possibility of Use of the MHD Control in Scramjet," AIAA Paper 99-4971, Nov. 1999.

[15] Bityurin, V. A., Klimov, A. I., Leonov, S. B., Bocharov, A. N., and Lineberry, J. T., "Assessment of a Concept of Advanced Flow/Flight Control for Hypersonic Flights in Atmosphere," AIAA Paper 99-4820, Nov. 1999.

[16] Chase, R. L., Mehta, U. B., Bogdanoff, D. W., Park, C., Lawrence, S., Aftosmis, M., Macheret, S. O., and Shneider, M. N., "Comments on an MHD Energy Bypass Engine Powered Spaceliner," AIAA Paper 99-4965, Nov. 1999.

[17] Park, C., Mehta, U. B., and Bogdanoff, D. W., "Real Gas Calculation of the MHD-Bypass Scramjet Performance," AIAA Paper 2000-3702, July 2000.

[18] Kuranov, A. L., and Sheikin, E. G., "Magnetohydrodynamics Control on Hypersonic Aircraft Under 'Ajax' Concept," *Journal of Spacecraft and Rockets*, Vol. 40, No. 2, 2003, pp. 174–182.

[19] Kurziner, R. I., *Jet Engines for Large Supersonic Flight Velocities*, Mashinostroenie, Moscow, 1989, p. 263.

[20] Sheikin, Y. G., "Analytical Solution for the Set of the MHD Equations in Quasi-1D Approximation for the Modes with Monotonic Variation of the Flow Parameters Lengthwise of the Channel 1," *Journal of Technical Physics*, Vol. 66, No. 12, 1992, pp. 1–8.

[21] Sheikin, Y. G., "Analytical Solution for the Set of the MHD Equations in Quasi-1D Approximation for the Modes with Monotonic Variation of the Flow Parameters Lengthwise of the Channel 2," *Journal of Technical Physics*, Vol. 67, No. 9, 1992, pp. 6–16.

[22] Brichkin, D. I., Kuranov, A. L., and Sheikin, E. G., "MHD Technology for Scramjet Control," 8th International Space Planes and Hypersonic Systems and Technologies Conference, Norfolk, VA, AIAA Paper 1998-1642, Apr. 1998.

[23] Curan, E. T., Leingang, J., Carreiro, L., and Peters, D., "Further Studies of Kinetic Energy Methods in High Speed Ramjet Cycle Analysis," AIAA Paper 92-3805, 1992.

[24] Berlyand, A. T., and Penzin, V. I., "Planar Flow over Multi-Stage Inlet by Hypersonic Flux of Ideal Gas," TsAGI, Preprint No. 11, Moscow, 1990, p. 20.

[25] Brichkin, D. I., Kuranov, A. L., and Sheikin, E. G., "The Potentialities of the MHD Control for Improving Scramjet Performance," 9th International Space Planes and Hypersonic Systems and Technologies Conference, Norfolk, VA, AIAA Paper 99-4969, Nov. 1999.

[26] Brichkin, D. I., Kuranov, A. L., and Sheikin, E. G., "Scramjet with MHD Control Under 'Ajax' Concept: Physical Limitations," 39th AIAA Aerospace Sciences Meeting, Reno, NV, AIAA Paper 2001-0381, Jan. 2001.

[27] Kuranov, A. L., and Asanova, R. Z., "Calculation of Electrokinetic Parameters of Air and Nitrogen Plasma Excited by Electron Beam," Hypersonic Systems Research Inst., St. Petersburg, Russia, 1995.

[28] Macheret, S. O., Shneider, M. N., and Miles, R. B., "Energy-Efficient Generation of Nonequilibrium Plasmas and Their Applications to Hypersonic MHD Systems," AIAA Paper 2001-2880, 2001.

[29] Golovachev, Yu. P., and Suschikh, S. Yu., "Weakly Ionized Flows in Supersonic Inlets Subjected to the External Electromagnetic Fields," *Perspectives of the MHD and Plasma Technologies in Aerospace Applications*, IVTAN, Moscow, Mar. 1999, p. 105.

[30] Brichkin, D. I., Kuranov, A. L., and Sheikin, Y. G., "Utilization of the MHD Systems on Hypersonic Vehicles," *Perspectives of the MHD and Plasma Technologies in Aerospace Applications*, Inst. for High Temperatures, Russian Academy of Sciences, Moscow, 1999, p. 1.

[31] Macheret, S. O., Shneider, M. N., and Miles, R. B., "Magnetohydrodynamic Control of Hypersonic Flows and Scramjet Inlets Using Electron Beam Ionization," *AIAA Journal*, Vol. 40, No. 1, 2002, pp. 74–81. doi:10.2514/2.1616

[32] Macheret, S. O., Shneider, M. N., and Miles, R. B., "Magnetohydrodynamic Power Extraction from Cold Hypersonic Airflows with External Ionizers," *Journal of Propulsion and Power*, Vol. 18, No. 2, 2002, pp. 424–443. doi:10.2514/2.5951

[33] "Stopping Powers for Electrons and Positrons," International Commission on Radiation Units and Measurements Rept. 37, Bethesda, MD, Oct. 1984.

[34] Kuranov, A. L., Korabelnikov, A. V., Kuchinsky, V. V., and Sheikin, Y. G., "Present Status of the Developments and Perspective Research of Hypersonic technologies Under 'Ajax' Concept," *Proceedings of the 2nd Meeting on Magnetoplasma Aerodynamics in Aerospace Applications*, Inst. of High Temperatures, Russian Academy of Sciences, Moscow, 2000, p. 20.

[35] Kuranov, A. L., and Sheikin, Y. G., "Possibilities of the MHD Control in Hypersonic Ramjet," *2nd Workshop on Magneto- and Plasma-Aerodynamics for Aerospace Applications*, Inst. of High Temperatures, Russian Academy of Sciences, Moscow, 2000, p. 31.

[36] Breyev, V. V., Gubarev, A. V., and Panchenko, V. P., *Supersonic MHD Generators*, Energoatomizdat, Moscow, 1986, p. 239.

[37] Kuranov, A. L., and Sheikin, E. G., "MHD Control on Hypersonic Aircraft Under 'Ajax' Concept: Possibilities of the MHD Generator," 40th AIAA Aerospace Sciences Meeting, Reno, NV, AIAA Paper 2002-0490, January 2002.

[38] Kuranov, A. L., and Sheikin, E. G., "MHD Control by External and Internal Flows in Scramjet Under 'Ajax' Concept," 41st AIAA Aerospace Sciences Meeting–Weakly Ionized Gas Workshop, Reno, NV, AIAA Paper 2003-173, Jan. 2003.

[39] Kuranov, A. L., and Sheikin, Y. G., "Utilization of the MHD Systems on Hypersonic Vehicles," *Proceedings of the 3rd Meeting on Magnetoplasma Aerodynamics in Aerospace Applications*, Inst. of High Temperatures, Russian Academy of Sciences, Moscow, 2001, pp. 25–26.

S. Macheret
Associate Editor